The Journal of Chemical Physics

Bond energy of ThN^+: A guided ion beam and quantum chemical investigation of the reactions of thorium cation with N_2 and NO

Cite as: J. Chem. Phys. **151**, 034304 (2019); https://doi.org/10.1063/1.5111534
Submitted: 27 May 2019 . Accepted: 24 June 2019 . Published Online: 18 July 2019

Richard M. Cox, Arjun Kafle, P. B. Armentrout, and Kirk A. Peterson

The Journal of Chemical Physics ARTICLE scitation.org/journal/jcp

Bond energy of ThN^+: A guided ion beam and quantum chemical investigation of the reactions of thorium cation with N_2 and NO

Cite as: J. Chem. Phys. 151, 034304 (2019); doi: 10.1063/1.5111534
Submitted: 27 May 2019 • Accepted: 24 June 2019 •
Published Online: 18 July 2019

Richard M. Cox,[1,a)] Arjun Kafle,[1] P. B. Armentrout,[1,b)] and Kirk A. Peterson[2]

AFFILIATIONS

[1]Department of Chemistry, University of Utah, Salt Lake City, Utah 84112-0850, USA
[2]Department of Chemistry, Washington State University, Pullman, Washington 99164-4630, USA

[a)]**Present address:** Pacific Northwest National Laboratory, P.O. Box 999, Richland, WA 99352, USA
[b)]**Author to whom correspondence should be addressed:** armentrout@chem.utah.edu.

ABSTRACT

Kinetic-energy dependent reactions of Th^+ with N_2 and NO are studied using a guided ion beam tandem mass spectrometer. The formation of ThO^+ in the reaction of Th^+ with NO is observed to be exothermic and barrierless with a reaction efficiency at low energies of 0.91 ± 0.18. Formation of ThN^+ in the reactions of Th^+ with N_2 and NO is endothermic in both cases. The kinetic-energy dependent cross sections for formation of this product ion were evaluated to determine a 0 K bond dissociation energy (BDE) of $D_0(Th^+–N)$ = 6.51 ± 0.08 eV, the first direct measurement of this BDE. Additionally, the reactions were explored by quantum chemical calculations, including a full Feller-Peterson-Dixon composite approach with correlation contributions up to CCSDTQ for ThN and ThN^+, as well as more approximate CCSD(T) calculations where a semiempirical model was used to estimate spin-orbit energy contributions. The ThN^+ BDE is found to be larger than those of the transition metal congeners, TiN^+ along with estimated values for ZrN^+ and HfN^+, believed to be a result of the actinide contraction.

INTRODUCTION

The chemistry of actinides (An) is of strong interest because of their use in nuclear power and because of national security concerns; however, the radioactive nature of the actinide series makes them problematic to investigate thoroughly without specially dedicated laboratories (except Th and U). Therefore, application of theoretical methods to study these systems becomes desirable. Because these heavy metals involve extensive spin-orbit and relativistic effects, it is imperative that experimental benchmarks are available to evaluate potential basis sets and theoretical methods. Such benchmarks can be provided by gas-phase studies, which are absent solvent effects, thereby allowing direct comparison with the highest levels of theory possible. A number of experimental gas-phase studies of actinide systems are available,[1–18] as well as theoretical reports.[14–26] Comparisons between these reveal examples of discrepant experimental and theoretical results,[14,23,24] indicating a need for further development.

Many of these studies have involved oxidation reactions, and it has been demonstrated that there is a correlation between bond dissociation energies (BDEs) of AnO^{p+} (p = 0–2) and the promotion energy (E_p) of An^{p+} to the lowest level having a $6d^2$ configuration.[13] Th and Th^+ are unique among the actinides because they do not populate the $5f$-orbitals in their ground states such that they are often compared with the better understood transition metals. Th and Th^+ have $6d^27s^2$ and $6d^27s$ ground level configurations, respectively, whereas most An have ground state configurations of $5f^{n-3}6d7s^2$ or $5f^{n-2}7s^2$, and most An^+ are $5f^{n-2}7s^2$ and $5f^{n-1}7s$. In contrast to oxidations, nitridations are much less studied even though metal nitrides can be formed under high temperature

conditions in air (conditions that might be available in nuclear reactors). However, the most likely source of nitrides is ambient dinitrogen, where the bond is very strong, $D_0(N_2) = 9.7544 \pm 0.0004$ eV.[27] As metal nitride BDEs should typically be smaller than this, the formation of metal nitrides in experiments conducted at thermal energies is unlikely and has not been studied systematically (see below). In addition, actinide nitrides are of interest as they show promise as a fuel source for fast breeder reactors. Nevertheless, there is little thermodynamic data on actinide nitrides, as detailed below.

To overcome the experimental limitations of studies performed at thermal energies, the present study utilizes guided ion beam tandem mass spectrometry (GIBMS), which is able to control reactant energies over a large range (four orders of magnitude) of kinetic energies. This permits studies of the energy dependences of endothermic reactions, which can then be used to directly measure key thermodynamic information. Furthermore, no knowledge of product molecular parameters is needed, which often limits the accuracy of thermodynamic information obtained from high temperature mass spectrometry studies. Previously, MN^+ BDEs have successfully been measured using GIBMS for only a few transition metals using either ammonia as a reactant[28,29] or N_2.[30–32] An early ion beam study examined the reaction of uranium cations with N_2 to determine the UN^+ bond energy.[33] Limits on several metal nitride cation bond energies come from the observation that reaction (1) occurs at thermal energies in drift tube studies for $M^+ = Ti^+$, Zr^+, Nb^+, La^+, Ce^+, Ta^+, and Os^+,[34,35]

$$M^+ + N_2O \rightarrow MN^+ + NO, \quad (1)$$

which indicates that $D(M^+–N) > D_0(N–NO) = 4.925 \pm 0.001$ eV.[27] Likewise, this reaction has been observed for Ce^+, Th^+, U^+, and Np^+ in ion cyclotron resonance (ICR) mass spectrometry experiments[3,5] Notably, Santos *et al.* failed to observe formation of MN^+ with Th^+, U^+, Np^+, and Pu^+ reacting with NO,[5] as did Johnsen *et al.* for Th^+ in a drift tube mass spectrometer.[36] These failures could indicate that $D(M^+–N) < D_0(NO) = 6.4964 \pm 0.0007$ eV.[27] To measure the ThN^+ bond energy more directly, the present study analyzes the absolute kinetic energy dependent cross sections of the endothermic formation of ThN^+ in reactions of Th^+ with N_2 and NO as measured using GIBMS. We also compare theoretically derived BDEs to this experimental benchmark and compare this value with those of transition metal analogs.

Literature thermochemistry review

Prior results on ThN and ThN^+ are sparse. Early measurements include a determination of the gas-phase 0 K BDE of ThN as 5.94 ± 0.35 eV using high temperature (2700 K) mass spectrometry.[37] In matrix isolation experiments, the vibrational frequency of ThN was measured as 934.3 cm^{-1} and density functional theory indicates that this species has a $^2\Sigma^+$ ground state, a vibrational frequency of 999 cm^{-1}, and a bond length of 1.795 Å.[38] More recently, laser induced fluorescence (LIF) and resonantly enhanced multiphoton ionization (REMPI) spectroscopy experiments by Heaven and co-workers confirm the $^2\Sigma^+$ ground state of ThN and measure a vibrational frequency of 950 ± 15 cm^{-1} and a rotational constant of 0.393 ± 0.002 cm^{-1}, which translates to a bond length of 1.80 ± 0.01 Å.[15] Their high-level MRCI+Q calculations indicate a vibrational frequency of 941.3 cm^{-1} and a bond length of 1.826 Å. Steimle and co-workers have spectroscopically characterized ThN obtaining a bond length of 1.822 22 Å, in good agreement with concomitant density functional theory (DFT) calculations.[39] Heaven and co-workers also examined ThN^+ using pulsed-field ionization zero kinetic energy (PFI-ZEKE) photoelectron spectroscopy.[15] There, an ionization energy of $IE(ThN) = 6.3272 \pm 0.0004$ eV and a rotational constant for ThN^+ of 0.410 ± 0.005 cm^{-1} (translating to a bond length of 1.76 ± 0.02 Å) were obtained and the ground state was spectroscopically confirmed to be $^1\Sigma^+$. Notably, the IE differs by only 0.020 eV from that of the atom, $IE(Th) = 6.306\,92 \pm 0.000\,01$ eV,[9,40,41] which means that the neutral and cationic BDEs differ by this amount as well. Given the BDE of ThN above, this suggests that $D_0(Th^+–N) = 5.92 \pm 0.35$ eV. This value is consistent with the lower limit of $D_0(Th^+–N) > D_0(N–NO) = 4.925$ eV noted above and with the failure to observe formation of ThN^+ in the reaction of Th^+ with NO, suggesting $D_0(Th^+–N) < D_0(NO) = 6.50$ eV (although such a failure can also be a result of kinetic limitations). Calculations indicate that all excited states of ThN^+ are relatively high in energy (>1.5 eV) because they must involve excitation of a bonding electron to a nonbonding orbital.

EXPERIMENTAL AND THEORETICAL METHODS

Instrument

The GIBMS used in these experiments has been described in detail previously.[42] Briefly, ions were created in a direct current discharge/flow tube source (DC/FT) described in more detail below.[43] After exiting the source, ions were focused through a magnetic momentum analyzer where the reactant $^{232}Th^+$ ion beam was mass selected. These ions were decelerated to a well-defined kinetic energy and passed into a radio frequency (rf) octopole ion guide[44,45] that constrained the ions radially. The octopole passed through a static pressure reaction cell that contained the neutral reaction partner (N_2 or NO). To ensure that the probability of multiple collisions between Th^+ and the neutral gas was sufficiently small, the pressure in the reaction cell was maintained at typical pressures of 0.10–0.40 mTorr. Measurements at several pressures were performed to ensure that measured cross sections are independent of neutral reactant pressures. Reaction cross sections were calculated from product ion intensities relative to reactant ion intensities after correcting for background ion intensities measured when the neutral gas was no longer directed into the gas cell.[46] Uncertainties in the calculated absolute cross section were estimated to be ±20%, with relative uncertainties of ±5%.

Laboratory ion energies (lab) were converted to the center-of-mass frame (CM) using the relationship $E_{CM} = E_{lab} \times m/(m + M)$, where m and M are the masses of the neutral reactant and ion, respectively. At very low energies, the conversion included a correction for the truncation of the ion kinetic energy distribution as described previously.[46] Cross sections are known to be broadened by the kinetic energy distribution of the reactant ions and the thermal (300 K) motion of the neutral reactant.[47] The absolute zero of energy and the full width at half-maximum (fwhm) of the ion beam were determined by using the octopole guide as a retarding potential analyzer.[46] Typical fwhms of the energy distribution for these

experiments were 0.4–0.6 eV (lab). Uncertainties in the absolute energy scale are 0.1 eV (lab). All energies reported below are in the CM frame.

Ion source

The DC/FT source has been described in detail previously.[43] Briefly, a cathode containing the thorium sample (^{232}Th, 100% abundance) was held at ~2.5 kV. The resultant electric field ionized Ar gas that flowed over the cathode in a 9:1 He/Ar mixture. The ionized Ar collided with the cathode, and Th^+ ions were sputtered off and swept into the flow tube by the He/Ar flow at typical pressures of 0.3–0.4 Torr. In the flow tube, ions were thermalized by ~10^5 collisions with carrier gas. In this work and previous work with Th^+,[16–18,48] there was no evidence of excited state species. Previous experiments[49–53] utilizing the DC/FT source with transition metal ions have indicated that the effective electronic energy of atomic ions can be characterized by temperatures of 300–1100 K. A population analysis at 300 K indicates that 99.89% of Th^+ is in its ground level ($^4F_{3/2}$, $6d^27s$), whereas at 1100 K, 76% is in the ground level.[41,54] Conservatively, we estimate the internal temperature to be 700 ± 400 K, where Th^+ has an average electronic energy of E_{el} = 0.02 ± 0.03 eV. The average excitation energy and its uncertainty are incorporated into all threshold and bond dissociation energies reported here.

Data analysis

The kinetic energy dependence of endothermic reactions was modeled using Eq. (2),[45,55,56]

$$\sigma(E) = \sigma_0 \sum g_i (E + E_{el} + E_i - E_0)^n / E, \quad (2)$$

where σ_0 is an energy-independent scaling factor, E is the relative kinetic energy of the reactants, E_i is the internal energy of the neutral reactants having populations g_i ($\Sigma g_i = 1$), n is an adjustable parameter, and E_0 is the 0 K reaction threshold. Before comparison to the data, Eq. (2) was convoluted over the kinetic energy distributions of the reactants, and the σ_0, n, and E_0 parameters were optimized using a nonlinear least-squares method to best reproduce the experimental cross section.[46,57] Uncertainties in E_0 were calculated from the threshold values from several independent data sets over a range of acceptable n values and combined with the absolute uncertainties in the kinetic energy scale and internal energies of reactant ions (E_{el} = 0.02 ± 0.03 eV). At high energies, cross sections decline because of product dissociation, so Eq. (2) was modified to include a statistical model of the dissociation probability, as discussed in detail elsewhere.[58] Briefly, the dissociation probability is controlled by two adjustable parameters: p, which is similar to n, but can hold only integer values, and E_d, the energy at which product cross sections begin to decline.

E_0 obtained from Eq. (2) is used to determine $D_0(Th^+–N)$ using Eq. (3), where L = N or O,

$$D_0(Th^+ - N) = D_0(N - L) - E_0. \quad (3)$$

Equation (3) assumes that there are no barriers in excess of the endothermicity of the reaction. No experimental evidence was found to suggest that such a barrier is present in either system studied here, and potential energy surfaces presented below are consistent with no barriers being present. For the neutral thermochemistry, we use values from the Active Thermochemical Tables (ATcT) of $D_0(N_2)$ = 9.7544 ± 0.0004 eV and $D_0(NO)$ = 6.4964 ± 0.0007 eV.[27]

Theoretical calculations

The majority of the quantum chemical calculations were performed using the Gaussian 09 suite of programs.[59] For Th^+, a polarized correlation consistent core-valence quadruple-ζ (20s17p12d11f7g4h1i)/[9s9p8d8f7g4h1i] basis set[60] was used with the Stuttgart-Cologne (MDF) small core (60 electron) relativistic effective core potential[61] (ECP), cc-pwCVQZ-PP. The cc-pwCVTZ-PP[60] basis set was also used in combination with the MDF ECP. Additionally, Stuttgart-Dresden (SDD-VDZ-MWB) and segmented quadruple-ζ (Seg. SDD-VQZ-MWB) were used in combination with the Stuttgart-Dresden small core quasirelativistic ECP (MWB).[62,63] The cc-pVXZ,[64] aug-cc-pwCVQZ,[65] cc-pwCVXZ (X = T, Q),[66] and Pople[67] 6-311 + G(3df) basis set were used for N. Extrapolation to the complete basis set limit (CBS) for the cc-pwCVXZ (X = T, Q) basis sets was performed using the Karton-Martin method[68] [Eq. (4)], for HF energies (where Y = 3 for T and Y = 4 for Q),

$$E_X = E_{CBS} + A(Y + 1)e^{-6.57\sqrt{Y}}. \quad (4)$$

For CCSD(T)/cc-pwCVXZ calculations, Eq. (5)[69] was used to extrapolate the correlation energy,

$$E_X = E_{CBS} + B(Y + 1/2)^{-4}. \quad (5)$$

The use of these basis sets has previously yielded reasonable results for other Th^+ and Th systems.[16,17,60,70–72]

Structures were optimized using density functional theory (DFT) functionals, B3LYP,[73,74] B3PW91,[75] BHandHLYP (BHLYP),[73] M06,[76] and PBE0[77] with unrestricted wavefunctions. B3LYP and B3PW91 have proven reliable in actinide theoretical calculations by us and others.[16,17,24,78] PBE0 and M06 have also yielded reasonable results, and M06 was indicated as a promising functional in studies of the ThO_2^+ BDE.[26] BHLYP has previously performed well in actinide systems when the molecule is singly bound[16,17] but performs poorly in systems with higher bond orders.[16,79] Nevertheless, it is included here because it performs well in predicting the energy spacing between electronic states of Th^+.[16,17] Additionally, single point energies using a spin unrestricted coupled cluster method that include single and double excitations and perturbative triple excitations, U/UCCSD(T),[80–83] were performed using the B3LYP optimized structures. For electron correlation calculations using U/UCCSD(T), the Th^+ 5s and 5p and the N 1s electrons are frozen. Electronically excited states of different spin and orbital angular momentum were calculated by explicitly manipulating the orbital occupations. All energies discussed below are corrected by the zero-point energy (ZPE) using the harmonic frequencies generated at their respective optimized structure after scaling by 0.989.[84] Potential energy surfaces were generated by performing relaxed potential scans along the $\angle LThN^+$ coordinate (L = N or O).

For the above theoretically calculated BDEs, a semiempirical approach that corrects for spin-orbit (SO) splitting was employed. This model is described in detail elsewhere.[16,85–87] Briefly, the uncor-

rected theoretical BDE is a value averaged over all spin-orbit states of the molecule and the dissociation asymptote. To correct for the SO splitting of the Th^+ + L asymptote, the contributions of L are considered negligible, and contributions of Th^+ are corrected by the difference in energy of the ground level and the energy of the ground state averaged over all SO levels. For Th^+, the J = 3/2 ground level is a mixture of the $^4F_{3/2}$ and $^2D_{3/2}$ levels. For the purpose of comparing experimental energies to theoretical energies, we have previously assigned the ground level as $^4F_{3/2}$.[16] Experimentally, the $^4F_{3/2}$ ground level lies 0.40 eV below the SO averaged ^2D ground state, which lies 0.06 eV below the SO averaged ^4F state. For ThN^+, the ground state is $^1\Sigma^+$ and hence has no first-order SO splitting such that no additional correction is necessary although this ignores any potential second-order effects from interacting states. For ThN^+, potential interacting states are separated sufficiently in energy that second-order effects are not believed to be significant.[15] Furthermore, the empirical spin-orbit correction used here (0.40 eV) is comparable to the spin-orbit contributions calculated using a composite thermochemistry approach described below (0.45 eV).

Composite thermochemistry with explicit spin-orbit calculations

Accurate composite thermochemistry, as outlined in the Feller-Peterson-Dixon method (FPD),[88–90] was used to describe the numerous contributions to the atomization energies at 0 K for ThN^+ and ThN. The majority of these calculations were carried out at the CCSD(T) level of theory with the third order Douglas-Kroll-Hess (DKH3) Hamiltonian[91,92] utilizing aug-cc-pVXZ-DK basis sets[64,65,93] on the N atom and the all-electron cc-pVXZ-DK3 basis sets on Th (X = D, T, Q)[60,90] (denoted cc-pVXZ-DK3 below). Core-valence correlation (1*s* on N with 5*s*5*p*5*d* on Th) was also considered, and in these cases, the aug-cc-pwCVXZ-DK (N)[66] and cc-pwCVXZ-DK3 (Th)[60] basis sets were used. Geometries were optimized at the frozen-core CCSD(T)/cc-pVQZ-DK3 level of theory and were consistently used as the reference geometries for all single point calculations except in the case of the ZPE described below. Open-shell calculations employed restricted open-shell HF (ROHF) orbitals, but the spin restriction was relaxed in the CCSD(T) calculations, i.e., the R/UCCSD(T) method[94–96] was used. Because of the highly multireference character of the $^4F_{3/2}$ ground state of Th^+ when SO is included, all dissociation energy calculations below were carried out relative to the ground electronic state of neutral Th atom ($^3F_2$). The calculated dissociation energies of ThN^+ were then corrected to the ground state of the Th^+ cation using the accurate experimental ionization energy (IE) of Th atom (6.306 92 eV).[9] All of these calculations, excluding the SO contributions, were carried out using the MOLPRO quantum chemistry package.[97]

The final FPD calculated dissociation enthalpies at 0 K consisted of the following contributions:

$$D_0 = E_{VQZ-DK3} + \Delta E_{CBS} + \Delta E_{CV} + \Delta E_{SO} + \Delta E_{QED} + \Delta E_{Gaunt} + \Delta E_T + \Delta E_Q + \Delta E_{IE} + \Delta E_{ZPE}, \quad (6)$$

where $E_{VQZ-DK3}$ is the equilibrium dissociation energy at the frozen-core CCSD(T)/cc-pVQZ-DK3 level of theory. The HF energies were then extrapolated to the CBS limit using Eq. (4) with cc-pVTZ-DK3 and cc-pVQZ-DK3 basis sets, while the correlation energies were extrapolated to their CBS limits using Eq. (5). The results of these two extrapolations for the molecules and atoms were combined to yield the total CBS limit dissociation energies, with the difference between the latter values and $E_{VQZ-DK3}$ yielding ΔE_{CBS}. ΔE_{CV} is the core correlation contribution, $E_{CV} - E_{valence}$, both in the same cc-pwCVXZ-DK3 basis sets (X = T and Q), extrapolated to the CBS limit using Eq. (5). The value of E_{CV} was obtained by correlating the 5s, 5p, and 5d electrons of Th and the 1s electrons of N in addition to the valence electrons.

SO contributions, ΔE_{SO}, were calculated using full 4-component Dirac-Hartree-Fock CCSD(T) with the Dirac-Coulomb Hamiltonian[98,99] and uncontracted cc-pVDZ-DK3 basis sets. The spin-free Hamiltonian of Dyall[100] was used for comparison. The contributions from the 2-electron Gaunt term, ΔE_{Gaunt}, were obtained at the 4-component DHF level with the Dirac-Coulomb-Gaunt Hamiltonian. The open-shell calculations for the Th atom utilized average-of-configuration HF orbitals (2 electrons in the 10 spinors arising from the 6d orbitals). All SO calculations involving coupled cluster correlated only the valence electrons and were carried out using a virtual orbital cutoff of 12.0 a.u. The SO calculations were carried out using the DIRAC program.[101] The SO contributions for the N(^4S) atom were taken to be zero.

ΔE_{QED} is a contribution for quantum electrodynamic effects (QED), namely, the Lamb shift. When considering molecules that contain heavy atoms such as actinides, this contribution can begin to become significant.[102] In this work, the local potential approach of Pyykkö was used for both the vacuum polarization and self-energy contributions.[60,103] The latter were carried out with the MOLPRO program at the frozen-core CCSD(T) level of theory with the cc-pwCVDZ-DK3 basis sets at the frozen-core cc-pVQZ-DK3 geometries.

The next two terms, ΔE_T and ΔE_Q, account for valence electron correlation effects beyond the CCSD(T) level of theory. The ΔE_T term is defined as the difference between CCSDT[94,104,105] and CCSD(T) in the cc-pVTZ-DK3 basis set with the DKH3 Hamiltonian. The effects of quadruple excitations, ΔE_Q, were defined as the difference between CCSDTQ[106–109] and CCSDT using cc-pVDZ-DK3 basis sets. The CCSDTQ/cc-pVDZ-DK3 calculations on ThN involved just under 3.4×10^9 configurations. The MRCC program[110] as interfaced to MOLPRO was used for all the higher-order electron correlation calculations. After correcting the dissociation energies of ThN^+ to the Th^+ dissociation asymptote using the experimental IE of Th,[9] ΔE_{IE}, harmonic frequencies at the frozen-core CCSD(T)/cc-pVDZ-DK3 level of theory were used to define the ZPE of each molecule, yielding ΔE_{ZPE}.

RESULTS

$Th^+ + N_2$ experimental results

The cross sections as a function of kinetic energy for the reaction of thorium cation with molecular nitrogen at a pressure of 0.4 mTorr are presented in Fig. 1. Reaction (7) was observed,

$$Th^+ + N_2 \rightarrow ThN^+ + N, \quad (7)$$

The reaction appears endothermic with an apparent threshold near 3 eV and a cross section that increases with increasing energy until it

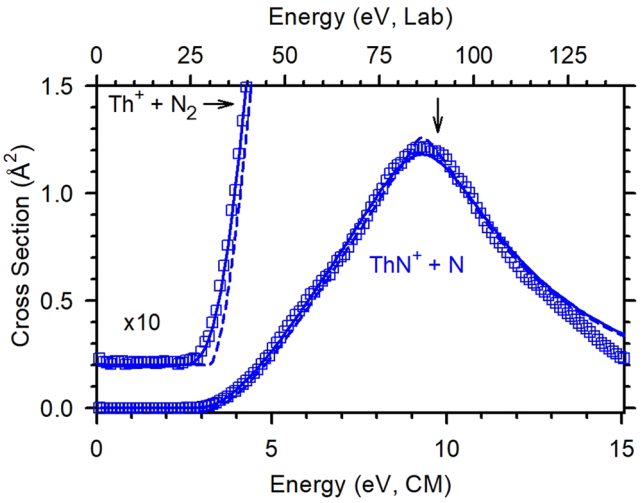

FIG. 1. Absolute cross sections for reaction of $Th^+ + N_2$ as a function of kinetic energy in the laboratory (upper x-axis) and center-of-mass (lower x-axis) frames. Lines show the model cross sections of Eq. (2), convoluted over the reactant internal and kinetic energy distributions (solid lines) and unconvoluted (dashed lines). The inset shows the data and models expanded by a factor of 10 and offset from zero by 0.2 Å^2. The arrow shows D_0(N–N) = 9.75 eV.

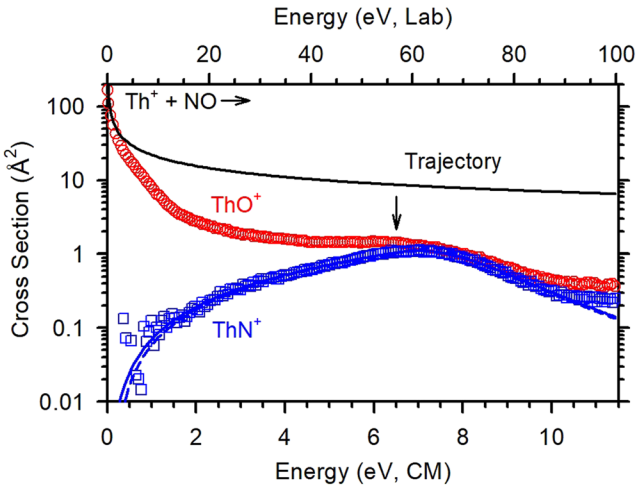

FIG. 2. Absolute cross sections for reaction of Th^+ + NO as a function of kinetic energy in the laboratory (upper x-axis) and center-of-mass (lower x-axis) frames. The solid black line represents the trajectory model of the collision limit. Blue lines show the model cross sections of Eq. (2), convoluted over the reactant internal and kinetic energy distributions (solid lines) and unconvoluted (dashed lines). The arrow shows D_0(N–O) = 6.50 eV.

peaks near $D_0(N_2)$ = 9.75 eV. At this point, sufficient energy is available to allow the ThN^+ product to dissociate, equivalent to atomizing N_2 according to reaction (8),

$$Th^+ + N_2 \rightarrow Th^+ + N + N. \quad (8)$$

Th^+ + NO experimental results

The cross sections of the reaction of Th^+ with NO as a function of kinetic energy are presented in Fig. 2. Both reactions (9) and (10) are observed,

$$Th^+ + NO \rightarrow ThO^+ + N, \quad (9)$$

$$\rightarrow ThN^+ + O. \quad (10)$$

The cross section for reaction (9) decreases with increasing energy, consistent with an exothermic, barrierless reaction. At low energies, the reaction efficiency is σ/σ_{Traj} = 0.91 ± 0.18, where the collision limit, σ_{Traj}, is the trajectory calculation for polar molecules of Su,[111] calculated using α = 1.70 Å^3 and μ = 0.16 D.[112] The cross section at low energies can be converted to a rate constant of 5.5 ± 1.1 × 10^{-10} cm^3/s, which compares well with that measured previously by Johnsen *et al.*, 7 ± 1.5 × 10^{-10} cm^3/s.[36] (Notably, the trajectory calculation indicates that the collision rate is 6.0 × 10^{-10} cm^3/s.) The cross section declines with an energy dependence of $E^{-0.5\pm0.1}$, consistent with the energy dependence ($E^{-1/2}$) of the trajectory cross section (σ_{Traj}) until approximately 0.2 eV where it begins to decline more rapidly until it levels out from 4 to 6 eV. This decline in the intermediate region can probably be attributed to the rate-limiting step in the reaction moving from the entrance channel (which controls σ_{Traj}) to the product channel. Although the product channel is much lower in energy (exothermic by 2.07 eV, see below), this shift occurs because the reduced mass of the products (μ′ = 13.3 amu) is much smaller than that of the reactants (μ = 26.6 amu) such that conservation of orbital angular momentum leads to a more rapidly increasing centrifugal barrier in the product channel with increasing energy.[113] At energies above 6 eV, the cross section begins to decline more rapidly, which can be attributed to there being sufficient energy present to dissociate the ThO^+ product, a process that can begin at D_0(N–O) = 6.50 eV.

The cross section for the ThN^+ product in reaction (10) is complicated by a small amount of mass overlap with the much more intense ThO^+ product. In the cross section shown, this has been subtracted out leading to a ThN^+ cross section that increases with increasing energy, indicating an endothermic reaction. This endothermicity is consistent with the failure to observe this process in ICR and drift tube studies at thermal energies.[5,36] The cross section rises monotonically until it reaches a maximum near D_0(NO), at which point there is sufficient energy for the ThN^+ product to begin to dissociate. Interestingly, the magnitude and shape of the ThO^+ and ThN^+ cross sections are very similar above this energy.

ThO^+ thermochemistry

In previous work, we have measured $D_0(Th^+–O)$ = 8.57 ± 0.14 eV from analysis of the reaction of Th^+ with CO.[18] As this BDE exceeds D_0(NO) = 6.50 eV, reaction (9) is exothermic by 2.07 eV, consistent with the behavior displayed in Fig. 2. Pulsed field ionization-zero kinetic energy (PFI-ZEKE) photoelectron spectroscopy experiments have determined a $^2\Sigma^+$ ground state for ThO^+ with a bond length of 1.807 Å and vibrational frequency of 955 cm^{-1}.[9] Theory indicates that this state has a $(1\sigma)^2(2\sigma)^2(1\pi)^4(3\sigma)^1$ molecular orbital occupation, where the 1σ-orbital is the O 2*s*-orbital, and the 2σ- and 1π-bonding orbitals

TABLE I. Fitting parameters from Eq. (2) for the indicated reaction cross section.

Reaction	n	σ_0	E_0 (eV)	$D_0(Th^+–N)$
$Th^+ + N_2 \rightarrow ThN^+ + N$	1.9 ± 0.2	0.4 ± 0.2	3.21 ± 0.20	6.54 ± 0.20
$Th^+ + NO \rightarrow ThN^+ + O$	2.5 ± 0.2	0.07 ± 0.03	$0.02^{+0.18}_{-0.02}$	$6.48^{+0.02}_{-0.18}$

are formed by combining O 2*p* and Th^+ 6*d* orbitals. The radical electron is found in the 3σ-orbital, which is largely composed of the Th^+ 7*s*-orbital, indicating that the $^2\Sigma^+$ state forms from the atomic asymptote, Th^+ (^{4}F, $6d^27s$) + O (^{3}P), a major component of the J = 3/2 ground level configuration. Bond lengths and vibrational frequencies calculated using B3LYP/cc-pwCVQZ-PP/aug-cc-pwCVQZ yielded molecular parameters that agree very well with experimental values: a bond length of 1.808 Å and a calculated vibrational frequency of 950 cm^{-1}.[18] This level of theory provided a 0 K BDE of 8.70 eV, which was matched by CCSD(T) calculations using the same basis set. The FPD approach yielded a BDE of 8.68 eV, within the uncertainty of the experimental value.[18]

ThN^+ thermochemistry

The cross sections for formation of ThN^+ in reactions (7) and (10) can be modeled using Eq. (2). These models are shown in Figs. 1 and 2, where it can be seen that they reproduce the cross sections with fidelity throughout the threshold region. As noted above, above the dissociation energy of the neutral, Eq. (2) is modified to include a dissociation probability, and it can be seen that these models also match the experimental results well for extended energy ranges. The parameters of Eq. (2) used in these models are given in Table I. For reaction (7), the E_0 value of 3.21 ± 0.20 eV can be combined with $D_0(N_2)$ = 9.7544 eV in Eq. (3) to provide $D_0(Th^+–N)$ = 6.54 ± 0.20 eV. For reaction (10), the best E_0 value is 0.02 eV, which can range up to 0.20 eV and down to nearly zero (0.001 eV) while still reproducing the data well. Independent of the modeling, the cross sections clearly suggest that reaction (10) is endothermic, even if only slightly, as do the ICR and drift tube experiments.[5,36] Combined with $D_0(NO)$ = 6.4964 eV, we take this threshold measurement to indicate that $D_0(Th^+–N)$ = 6.48 ± 0.18 eV, in good agreement with the result from the N_2 reaction. A weighted average of 6.54 ± 0.20 and 6.48 ± 0.18 eV yields $D_0(Th^+–N)$ = 6.51 ± 0.08 eV, where the uncertainty is two weighted standard deviations. This value properly reflects the likely endothermicity of reaction (10).

To the best of our knowledge, there are no direct determinations of the ThN^+ BDE in the literature. As described above, a value of $D_0(Th^+–N)$ = 5.92 ± 0.35 eV can be calculated from the neutral ThN BDE evaluated in high temperature mass spectrometry experiments[37] combined with the IEs of Th and ThN.[9,15] This value is somewhat lower than that obtained here. Likely reasons for the discrepancies are the assumptions made in extrapolating the high temperature results (near 2700 K) down to 0 K. We can combine our present ThN^+ BDE with the precisely known IE(Th) and IE(ThN) to yield a better estimate of $D_0(ThN)$ as 6.53 ± 0.08 eV.

ThN^+ theoretical results

A summary of our theoretical calculations on ThN^+ is provided in Table II. Here, the 1σ orbital is primarily composed of the N 2*s* orbital, the 2σ and 1π orbitals are bonding interactions between the N 2*p* and Th^+ 6*d*, the 3σ orbital is primarily the Th^+ 7*s* orbital, the 1δ orbital is the remaining Th^+ 6*d* orbitals, and the 4σ and 2π orbitals are the antibonding interactions corresponding to the 2σ and 1π orbitals. These establish a triply bonded $^1\Sigma^+$ with a $(1\sigma)^2(2\sigma)^2(1\pi)^4$ configuration as the ground state of ThN^+. In agreement with the theoretical work of Heaven,[10] the lowest lying excited state is a $^3\Sigma^+$ excited state where one of the 2σ bonding electrons is promoted to the 3σ orbital. This state is found to lie 1.06–1.62 eV above the ground state, comparable to an excitation of ~1.4 eV calculated by Heaven *et al.* These authors note that the associated $^1\Sigma^+$ $(1\sigma)^2(2\sigma)^1(1\pi)^4(3\sigma)^1$ state lies only slightly higher in energy. If the promotion occurs to a 1δ orbital instead, the $^3\Delta$ state is

TABLE II. Bond lengths (Å), vibrational frequencies (cm^{-1}), and relative energies (in eV) of low lying states of ThN^+.[a]

State	$r(Th^+–N)$[b]	ν[b]	CCSD(T)	B3LYP	B3PW91	M06	BHLYP	PBE0
$^1\Sigma^+$ $(1\sigma^21\pi^42\sigma^2)$	1.78(1.76)	1058 (1010)	0.00	0.00	0.00	0.00	0.00	0.00
$^3\Sigma^+$ $(1\sigma^21\pi^42\sigma3\sigma)$	1.87	913	1.40	1.20	1.30	1.62	1.28	1.06
$^3\Delta$ $(1\sigma^21\pi^42\sigma1\delta)$	1.89	869	1.96	1.68	1.69	1.93	1.52	1.67
$^3\Pi$ $(1\sigma^21\pi^32\sigma^23\sigma)$	1.95	833	2.13	1.83	1.99	2.27	1.71	1.98
$^5\Phi$ $(1\sigma^21\pi^32\sigma3\sigma1\delta)$	2.14	609	4.34	4.00	4.10	4.61	3.59	4.07

[a]Structure optimized at respective level of theory [except CCSD(T)] using cc-pVQZ-PP/6-311 + G(3df) basis sets.
[b]Bond lengths (in Å) or frequencies (in cm^{-1}) from B3LYP/cc-pVQZ-PP/6-311 + G(3df) optimized structures. Frequencies scaled by 0.989. Values in parentheses are experimental values from Ref. 10.

formed, 1.52–1.96 eV above the ground state (1.89 eV from Heaven *et al.*). Excitation of a bonding π-electron to the 3σ-orbital leads to the $^3\Pi$ excited state, 1.71–2.27 eV higher than the ground state (~2.2 eV from Heaven *et al.*). We also located a $^5\Phi$ state involving two excitations and hence a much higher excitation energy, 3.6–4.6 eV.

Interestingly, although ground state ThN^+ has a triple bond similar to ThO^+, the ThN^+ bond energy is 2 eV weaker than that of ThO^+. Importantly, ThO^+ ($^2\Sigma^+$, $1\sigma^2 2\sigma^2 1\pi^4 3\sigma$) can form directly from ground state Th^+ ($^4F_{3/2}$, $6d^2 7s$) and O (^3P, $2s^2 4p^4$). By contrast, coupling of ground state Th^+ and N (^4S, $2s^2 2p^3$) would lead to the first excited state ThN^+ ($^3\Sigma^+$, $1\sigma^2 1\pi^4 2\sigma 3\sigma$) with a bond order of 2.5. When accounting for the ~1.4 ± 0.2 eV excitation energy of the ground state to the $^3\Sigma^+$ state, the bond energy, $D_0(Th^+–N, {}^3\Sigma^+)$ = 5.1 ± 0.2 eV, is very similar to the BDE of ThC^+ ($^2\Sigma^+$, $1\sigma^2 1\pi^4 2\sigma$), $D_0(Th^+–C)$ = 4.82 ± 0.29 eV reported previously.[18] This is consistent with the nonbonding nature of the 3σ orbital. Diabatic formation of the $^1\Sigma^+$ ground state of ThN^+ requires that three unpaired 6*d*-orbital electrons be available to bond with the three unpaired 2*p*-electrons in the nitrogen to form the requisite triple bond. The first electronic level of Th^+ with three unpaired 6*d*-electrons available is the $^4F_{3/2}$ ($6d^3$) level that lies 0.87 eV above the ground level.[114] Assuming no secondary interactions, the diabatic BDE of the ThN^+ $^1\Sigma^+$ ground state can then be estimated as 7.38 ± 0.08 eV. This value is 1.2 eV lower than the ThO^+ bond energy, similar to the difference in the BDEs of N_2 and CO, 1.4 eV. Thus, the bond energy of ThN^+ is depressed by the cost of the excitation energy to the reactive ^4F ($6d^3$) state.

Our B3LYP/cc-pVQZ-PP/6-311 + G(3df) calculations find a bond length of 1.78 Å for the ground state, consistent with the spectroscopic results of Heaven.[10] B3LYP bond lengths for ThN^+ ground and excited states are listed in Table II. As can be expected, excitation of a bonding electron to a nonbonding orbital results in lengthening of the bond and a drop in the vibrational frequency, and the double excitation associated with the $^5\Phi$ state increases these changes even more. The bond lengths calculated here are in qualitative agreement with the potential energy surfaces for the $^3\Sigma^+$, $^3\Delta$, and $^3\Pi$ states shown by Heaven.[10]

Theoretical BDEs for ThN^+ are listed in Table III and range from 6.23 to 6.63 eV (SDD-VDZ-MWB), 6.15–6.76 eV (Seg. SDD-VDZ-MWB), 6.38–6.56 eV (cc-pwCVQZ-PP), 6.42–6.76 eV (CBS-PP), and 6.49 eV (FPD). In general, all levels of theory are in reasonable agreement with the experimental BDE with most values within 0.3 eV. In particular, the CCSD(T)/CBS-PP, PBE0/CBS-PP, and FPD results are rather accurate (as are several other determinations).

We can also compare these results to those for $ThCH^+$, isoelectronic with ThN^+. Here, the bond length was calculated as 1.92 Å (B3LYP/SDD-VDZ-MWB), longer than that of ThN^+, consistent with the weaker BDE, measured as $D_0(Th^+–CH)$ = 6.19 ± 0.16 eV.[16] Theoretical BDEs for ThN^+ are similar but systematically greater than those calculated for $ThCH^+$, 5.57–6.21 eV (Seg. SDD-VQZ-MWB).[16] This is consistent with a bond order of three in both molecules and with the relative values in the experimental determinations of both ThN^+ and $ThCH^+$.

ThN theoretical results

In order to calculate IE(ThN), additional calculations were performed for ThN using the B3LYP/cc-pwCVQZ-PP/aug-cc-pwCVQZ approach. Additional single point energies were calculated using CCSD(T)/cc-pwCVQZ-PP/aug-cc-pwCVQZ and its CBS extrapolation using the B3LYP optimized structures. As in the literature,[15] the ThN ground state is $^2\Sigma^+$ ($1\sigma^2 1\pi^4 2\sigma^2 3\sigma$), isoelectronic with ThO^+. Thus, the electron removed upon ionization of ThN is from the nonbonding 3σ (largely Th 7*s*) orbital, consistent with the observation that IE (ThN) ≈ IE(Th). Calculated IEs of ThN are 6.38 (B3LYP), 6.30 (CCSD(T)/VQZ), and 6.31 (CCSD(T)/CBS) eV, in good agreement with the 6.3272 ± 0.0004 eV experimental value determined by Heaven *et al.*[15]

TABLE III. Comparison of theoretical $D_0(Th^+–N)$ to experimental values (in eV).

Experimental			Theoretical[a]					
Literature	This work	Basis set	CCSD(T)[b]	B3LYP	B3PW91	PBE0	BHLYP	M06
5.92 ± 0.35[c]	6.51 ± 0.08	SDD	6.23	**6.45**	6.63		5.54	
≥4.925 ± 0.001[d]		Seg. SDD	6.15	**6.56**	6.76	6.73	5.66	6.91
≤6.4964 ± 0.0007[e]		cc-pwCVQZ-PP[f]	6.38	6.41	**6.53**	**6.56**	5.52	6.72
		CBS-PP[g]	**6.49**	6.42	6.76	**6.56**	5.52	6.68
		FPD[h]	**6.49**					

[a]From structures optimized at the respective level of theory [except CCSD(T)] with the indicated basis set. Energies include an estimated spin-orbit correction of −0.40 eV. See text and Ref. 16. Values in bold are within experimental uncertainty of the experimental value from the present work.
[b]Energies from single point calculations using B3LYP optimized structures with the indicated basis set for Th^+.
[c]Derived from $D_0(Th^+–N) = D_0(ThN) + IE(Th) - IE(ThN)$; see text.
[d]Lower limit from observation of reaction (1), Refs. 3 and 5.
[e]Upper limit from failure to observe formation of ThN^+ in reaction of Th^+ with NO, Refs. 5 and 36.
[f]cc-pwCVQZ-PP/aug-cc-pwcVQZ basis sets.
[g]Complete basis set limit extrapolated from pwCVXZ-PP/cc-pwCVXZ (X = T, Q) basis sets using Eqs. (4) and (5); see text.
[h]Feller-Peterson-Dixon model for composite thermochemistry. See text, Eq. (6), and Table IV.

TABLE IV. Calculated contributions to the dissociation energies within the FPD scheme in kJ/mol (eV). See Eq. (6) for details.

Molecule	$E_{VQZ\text{-}DK}$	ΔE_{CBS}	ΔE_{CV}	ΔE_{QED}	ΔE_{T}	ΔE_{Q}	ΔE_{SO}	ΔE_{Gaunt}	ΔE_{IE}	ΔE_{ZPE}	D_0
ThN^+	49.11	+11.24	+3.79	+3.98	−6.57	−0.06	−43.50	+5.36	608.53	−6.04	625.8
$(^1\Sigma^+)$[a]	(0.51)	(+0.12)	(+0.04)	(+0.04)	(−0.07)	(+0.00)	(−0.45)	(+0.06)	(6.31)	(−0.06)	(6.49)
ThN	653.00	+11.46	+7.32	+2.34	−7.12	+1.42	−39.74	+4.04	N/A	−5.63	627.1
$(^2\Sigma^+)$[b]	(6.77)	(+0.12)	(+0.08)	(+0.02)	(−0.07)	(+0.01)	(−0.41)	(+0.04)		(−0.06)	(6.50)[c]

[a] At a FC-CCSD(T)/cc-pVQZ-DK3 equilibrium bond length of 1.7906 Å. Combining the current results for ThN^+ and ThN yields a final FPD ionization energy at 0 K of 609.8 kJ/mol (6.320 eV).
[b] At a FC-CCSD(T)/cc-pVQZ-DK3 equilibrium bond length of 1.8282 Å.
[c] Using the experimental IEs of both ThN and Th atom, this yields $D_0(ThN^+)$ = 625.1 kJ/mol (6.48 eV).

Composite thermochemical calculations

In previous calculations of actinide species,[60] the FPD composite approach without any higher-order correlation contributions reproduced the atomization energies of ThO_2 and UF_n (n = 1–6) species within 0.05 eV of the mean experimental values. Furthermore, the BDEs of ThO^+ and ThC^+, which also included correlation contributions beyond just CCSD(T), were reproduced within the uncertainties of the experimental values.[18] Here, the details of the FPD results are displayed in Table IV. The value of IE(ThN) obtained from the composite FPD approach is calculated to be 6.320 eV, in excellent agreement with the accurately known experimental value of 6.3272 ± 0.0004 eV.[15] Furthermore, the composite $D_0(Th^+–N)$ value agrees very well with the experimental value reported here whether the theoretical or experimental IEs of Th and ThN are used, 6.49 and 6.48 eV, respectively. As with the calculations for ThO^+ and ThC^+, and as shown in Table IV for ThN and ThN^+, to confidently obtain an accuracy of a few kJ/mol, certainly CCSDT and also CCSDTQ calculations are necessary (although the Q contributions were small relative to CCSDT, this was not known *a priori*). Also shown in Table IV is the importance of the Lamb shift (QED) correction, which increased the BDEs by 2–4 kJ/mol. The Lamb shift is generally large when there is a change in *s* orbital occupation because these processes exhibit the largest effects of scalar relativity. For the present ThN^+ and ThN calculations, the BDE is computed relative to neutral Th atom, which has a $6d^27s^2$ electron configuration, whereas ThN^+ and ThN have nominal $7s^0$ and $7s^1$ occupations, respectively. Also shown in Table IV is the large impact of including SO coupling. This is almost entirely a result of the atomic SO of Th atom. As for transition metal species (see, for instance, Refs. 115–117), these results indicate that high level theoretical calculations are necessary to accurately reproduce experimental BDEs for actinide systems.

$Th^+ + N_2$ potential energy surfaces

Relaxed potential energy scans of the electronic surfaces for reaction (7), $Th^+ + N_2$, were calculated at the B3LYP/SDD-VDZ-MWB/6-311 + G(3df) level and are presented in Fig. 3 (where only species having C_{2v} or near C_{2v} symmetry are shown). These surfaces (as well as those for $Th^+ + NO$ below) do not include consideration of spin-orbit effects. Molecular parameters for the various intermediates on these surfaces can be found in Table V.

Ordinarily, dinitrogen binds to metal ions end-on in a linear geometry, but such an interaction with $Th^+(^2D)$ means that the dinitrogen electrons interact repulsively with the $7s^2$ orbital on $Th^+(^2D)$; hence, interaction with $Th^+(^4F, 6d^27s^1)$ is more favorable. Five linear $ThNN^+$ complexes were located lying 0.61–0.18 eV below the $Th^+(^2D) + N_2(^1\Sigma_g^+)$ asymptote. These all have NN bond lengths that are slightly extended (by 0.02–0.04 Å) compared to free N_2 (1.09 Å). If the dinitrogen interacts side-on with Th^+, several quartet and doublet species surfaces having potential wells near 30° were located. The lowest of these is a $^2A_1$ state (0.59 eV below reactants) with a NN bond length of 1.225 Å, suggesting that the Th has been inserted into the in-plane N_2 π bond (which is also consistent with the orbital character). Further insertion of Th^+ into the dinitrogen bond at larger ∠NThN bond angles of 40°–60° leads to barriers that lie about 3 eV above ground state reactants. Along the doublet

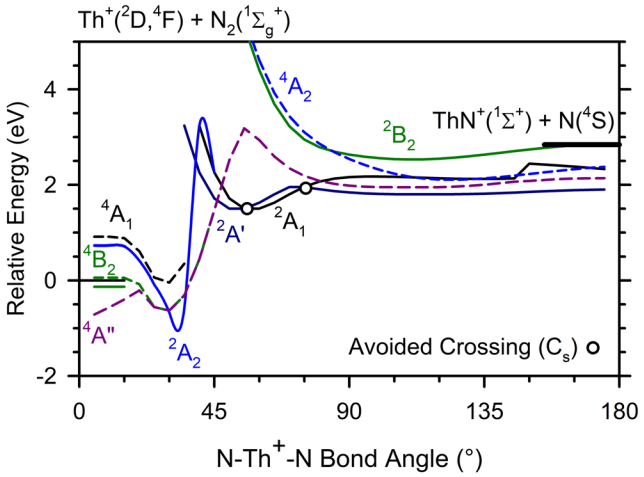

FIG. 3. B3LYP/SDD-VDZ-MWB/6-311 + G(3df) relaxed potential energy surface calculations of the $Th^+ + N_2$ reaction as a function of ∠NThN in degrees. Energies are relative to Th^+ (^2D, $6d7s^2$) + N_2. In C_{2v} symmetry, doublet surfaces are represented by solid lines and quartet surfaces by dashed lines. Surface crossings that are avoided in C_s symmetry are represented by open circles. Reactant and product energy levels are indicated by thick bars at 0° and 180°, respectively. No spin-orbit interactions are included.

TABLE V. Bond lengths (Å), bond angles (deg), vibrational frequencies (cm^{-1}), and energies of intermediates along the ThN_2^+ potential energy surfaces calculated at the B3LYP/SDD-VDZ-MWB/6-311+G(3df) level.

	r(ThN)[a]	r(N_2)	∠NThN	ν (cm^{-1})[a]	E (E_h)	ZPE (E_h)	E_{rel} (eV)
Th^+ (^{2}D)					−407.331 717		
N (^{4}S)					−54.600 723		
N_2 ($^1\Sigma_g^+$)		1.091		2446	−109.567 371	0.005 572	
$^2\Pi$	2.379, 3.492	1.112	0.0	200, 244, 264, 2110	−516.921 014	0.006 419	−0.534
$^2\Sigma^-$	2.308, 3.429	1.121	0.003	240, 264, 281, 2028	−516.912 296	0.006 411	−0.337
$^4\Sigma^-$	2.274, 3.398	1.124	0.0	224, 285(2), 1951	−516.922 280	0.006 255	−0.613
$^4\Delta$	2.261, 3.394	1.134	0.0	282, 304(2), 1867	−516.906 418	0.006 283	−0.180
$^4\Phi$	2.392, 3.506	1.114	0.0	199, 250, 267, 2089	−516.918 809	0.006 390	−0.515
$^4A''$	2.427, 2.426	1.156	27.6	178, 262, 1907	−516.912 807	0.005 346	−0.379
$^4B_1$	2.403(2)	1.158	27.9	174, 386, 1873	−516.918 054	0.005 543	−0.517
$^4B_2$	2.259(2)	1.213	31.2	352, 707, 1549	−516.894 039	0.005 942	0.147
$^4A_1$	2.224(2)	1.225	32.0	427, 434, 1570	−516.920 876	0.005 537	−0.594
$^2B_2$	2.199(2)	1.232	32.5	342, 354, 1462	−516.892 485	0.004 918	0.162
$^2A_2$	2.070(2)	1.318	37.1	271, 413, 1185	−516.911 341	0.004 258	−0.369
$^2A_1$	1.928(2)	1.853	57.4	486, 811, 835	−516.839 944	0.004 856	1.590
$^2B_1$	2.024(2)	1.952	57.7	325, 700, 745	−516.788 456	0.004 035	2.969
$^4A_1$	1.978(2)	2.806	90.3	178, 257, 775	−516.824 855	0.002 759	1.944
$^4A'$	2.011, 2.143	3.396	109.6	58, 206, 692	−516.798 208	0.002 177	2.654
$^2B_2$	1.950(2)	3.218	111.2	127, 681, 1000	−516.801 266	0.004 118	2.623
$^4A''$	1.886, 2.149	3.411	115.3	89, 450, 794	−516.822 784	0.003 039	2.008
$^2A_1$	1.926(2)	3.551	134.4	90, 698, 1020	−516.816 384	0.004 117	2.211
$^2A''$	1.876, 2.125	3.997	175.0	−36, 514, 834	−516.824 363	0.003 070	1.966
$^2\Pi$	1.929(2)	3.858	180.0	−25, 80, 746, 1429	−516.805 332	0.005 139	2.540
$^4\Sigma_u^+$	2.021(2)	4.042	180.0	−106(2), 543, 660	−516.797 067	0.002 742	2.700

[a]Degeneracies in parentheses.

surfaces, these lead to intermediates having bond angles of about 57° and NN distances of 1.85–1.95 Å such that the NN bond has essentially been cleaved. A series of both doublet and quartet dinitride intermediates having large ∠NThN bond angles (90°–134°) was also located (Table V). Linear $NThN^+$ species were located, but all had imaginary bending frequencies. The $NThN^+$ quartet intermediates should readily dissociate to the $ThN^+(^1\Sigma^+) + N(^4S)$ product asymptote, whereas dissociation of the more strongly bound doublet intermediates is spin-forbidden (although this may not be a restriction for such a heavy metal system). Overall, these surfaces show that reaction (7) can occur by insertion of the thorium cation into the dinitrogen bond with a barrier comparable to or slightly less than the endothermicity of reaction (7). Therefore, it seems possible that this reaction may also occur via more direct pathways in which the Th^+ strips one of the nitrogen atoms without actually forming an insertion intermediate.

If spin-orbit effects are considered, the only significant change to the surfaces is that the ground level of the reactants (and principally occupied level) becomes $Th^+(^4F_{3/2}) + N_2(^1\Sigma_g^+)$, which lies 0.40 eV lower than the ^{2}D state shown as the reactant asymptote at zero in Fig. 3. These reactants can combine to form quartet surfaces that lead to the final products. Because the J = 3/2 ground level also contains appreciable $^2D_{3/2}$ character, evolution along the doublet surfaces is also possible but requires formally converting back to a quartet surface upon product formation.

Th^+ + NO potential energy surfaces

Surfaces from relaxed potential surface scans calculated using B3LYP/SDD-VDZ-MWB/6-311 + G(3df) for reactions (9) and (10), Th^+ + NO, are presented in Fig. 4. Molecular parameters for the various intermediates on these surfaces can be found in Table VI. Covalent interaction of NO with $Th^+(^2D, 6d7s^2)$ leads to the singlet surface, $^1A'$, which shows minima at ∠NThO angles of 2° and 48°, which are both $ThNO^+$ geometries. There is also a shallow minimum at large angles that indicates an inserted $NThO^+$ geometry, and there is a $^1\Sigma^+$ state at 180° as well. Examination of the molecular orbitals here shows a $\sigma^2\pi^4\pi^4$ valence configuration such that the bond order between thorium (which uses three 6*d* orbitals) and each ligand is 2.5. Finally, a $ThON^+$ geometry having a bond angle of 6° was also located (Table VI) (not shown in Fig. 4).

We also located two triplet surfaces having A′ and A″ symmetry (there should be several more that our computational procedure will not locate). The $^3A'$ surface forms a bound species

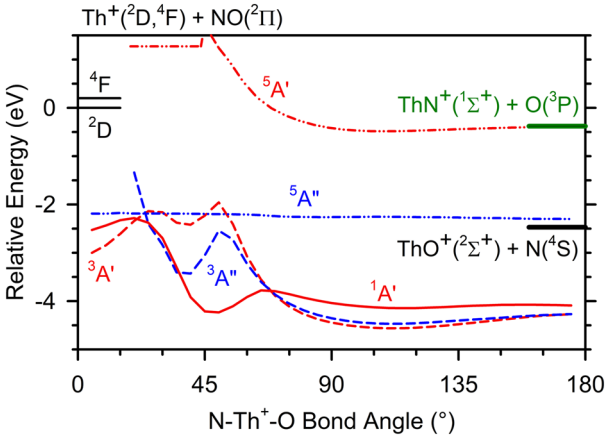

FIG. 4. B3LYP/SDD-VDZ-MWB/6-311 + G(3df) relaxed potential energy surface calculations of the Th^+ + NO reaction in C_s symmetry as a function of ∠NThO in degrees. Energies are relative to Th^+ (^{2}D, 6d7s^2) + NO. Singlet surfaces are represented by solid lines, triplet surfaces by dashed lines, and quintet surfaces by dashed-double dotted lines. Reactant and product energy levels are indicated by thick bars at 0° and 180°, respectively. No spin-orbit interactions are included.

at a linear $ThNO^+$ geometry that can be thought of as a covalent interaction of the NO singly occupied orbital (SOMO) with a singly occupied 6$d\pi$ orbital on Th^+(^{4}F), with the singly occupied orbitals being 7s and the other 6$d\pi$ (which interacts with the empty π^* orbital on NO). On both ^{3}A′ and ^{3}A″ surfaces, bound species are formed at angles near 38°. Here, the Th^+(^{4}F) state has been inserted into a π bond of NO such that the highest occupied orbitals are either $(1a')^1(2a')^1(1a'')^2$ or $(1a')^1(2a')^2(1a'')^1$ where 1a′ is largely 7s, 2a′ is an in-plane bonding interaction between NO(π^*) and Th^+(6$d\pi$), and 1a″ is an out-of-plane bonding interaction between NO(π^*) and Th^+(6$d\delta$). At still larger angles, both surfaces become nearly degenerate with minima near 112° converging to a degenerate $^3\Pi$ state at 180° (imaginary bending frequencies). The ^{3}A″ state at 112° is the global minimum on all potential energy surfaces (4.59 eV below reactants). Note that formation of either product asymptote, ThO^+($^2\Sigma^+$) + N(^{4}S) or ThN^+($^1\Sigma^+$) + O(^{3}P), can evolve from these triplet surfaces in spin-allowed reactions, whereas neither asymptote correlates diabatically with the singlet surface.

Interaction of NO with Th^+(^{4}F) can also lead to intermediates having quintet spin, but these are relatively high in energy. Indeed, the ^{5}A″ surface can be characterized as a nitrogen atom adduct of ThO^+, in which there is a high-spin interaction between the SOMO (largely 7s) on ThO^+ and the three p electrons on N. This also explains why there is little change in the energy of this state as the ∠OThN bond angle changes. The ^{5}A′ surface is much higher in energy because it decreases the bond order of the ThO bond from 3 to 2.5 (increasing the bond length from 1.8 to 2.1 Å) while making a covalent ThN bond (bond order of 1.5–2, decreasing the bond length from 2.9 to 2.1 Å).

Importantly, the formation of strongly bound $NThO^+$ intermediates can occur in a spin-allowed fashion from ground state

TABLE VI. Bond lengths (Å), bond angles (deg), vibrational frequencies (cm^{-1}), and energies of intermediates along the $ThNO^+$ potential energy surfaces calculated at the B3LYP/SDD-VDZ-MWB/6-311 + G(3df) level.

	r(ThN)	r(ThO)	r(NO)	∠NThO	ν (cm^{-1})[a]	E (E_h)	ZPE (E_h)	E_{rel} (eV)
O (^{3}P)						−75.090 913		
NO ($^2\Pi$)			1.145		1980	−129.939 901	0.004 510	
^{1}A′($ThNO^+$)	1.962	3.166	1.207	1.9	307, 536, 1497	−537.365 187	0.005 328	−2.524
$^3\Pi$ ($ThNO^+$)	1.999	3.207	1.209	0.0	305, 350, 515, 1428	−537.383 770	0.005 918	−3.014
$^5\Delta$ ($ThNO^+$)	2.197	3.370	1.173	0.0	251(2), 409, 1745	−537.364 701	0.006 050	−2.491
^{1}A′($ThON^+$)	3.271	2.084	1.217	6.0	142, 427, 1273	−537.291 137	0.004 196	−0.540
$^3\Pi$ ($ThON^+$)	3.385	2.107	1.278	0.0	184, 191, 446, 1113	−537.333 735	0.004 407	−1.693
$^5\Delta$ ($ThON^+$)	3.373	2.097	1.276	0.0	193(2), 449, 1100	−537.345 872	0.004 410	−2.023
^{3}A′	2.079	2.123	1.371	38.1	343, 598, 991	−537.361 012	0.004 400	−2.435
^{3}A″	2.123	2.103	1.362	37.6	457, 591, 1047	−537.399 418	0.004 772	−3.471
^{1}A′	1.947	1.966	1.590	47.9	457, 697, 852	−537.427 758	0.004 572	−4.247
^{5}A″	2.946	1.814	3.291	83.9	50, 118, 932	−537.354 720	0.002 508	−2.316
^{5}A′	2.133	2.125	3.459	108.7	85, 596, 600	−537.289 956	0.002 919	−0.542
^{3}A″	2.283	1.826	3.414	111.9	108, 456, 917	−537.435 917	0.003 371	−4.501
^{3}A′	2.140	1.829	3.303	112.4	110, 546, 905	−537.439 288	0.003 557	−4.588
^{1}A′	2.119	1.833	3.367	116.7	91, 496, 893	−537.423 997	0.003 372	−4.177
$^1\Sigma^+$	1.890	1.846	3.736	180.0	100(2), 769, 831	−537.421 502	0.004 101	−4.090
$^3\Pi$	2.163	1.826	3.989	180.0	−101, −81, 521, 889	−537.428 536	0.003 212	−4.305
$^5\Sigma^+$	3.079	1.815	4.894	180.0	31(2), 101, 934	−537.356 266	0.002 496	−2.358

[a]Degeneracies in parentheses.

reactants with no activation energy required. No barriers from these intermediates to either product asymptote exist such that the global minimum can readily dissociate to either $ThO^+(^2\Sigma^+)$ + $N(^4S)$ or $ThN^+(^1\Sigma^+)$ + $O(^3P)$ product asymptotes. If spin-orbit effects are considered, the Th^+ ($^4F_{3/2}$) reacts most readily with NO ($^2\Pi$) along a triplet spin surface. However, the J = 3/2 ground level is actually a mixture of $^4F_{3/2}$ and $^2D_{3/2}$ such that both singlet and triplet surfaces should be accessible in the reaction and that switching between surfaces of different spin is facile.

DISCUSSION

Comparison to other metal nitride cations

An interesting aspect of Th^+ is that unlike the other actinides, the 5*f*-orbitals are not populated in the ground level. This makes the comparison of the Th^+ chemistry to transition metal chemistry, which usually has been more thoroughly studied, especially fruitful. In our work on ThH^+, $ThCH_x^+$ (x = 0–3), and ThO^+,[17,18] we compared Th^+ to the group 4 transition metal ions, Ti^+, Zr^+, and Hf^+. Unfortunately, nitrides have been much less thoroughly studied than these other ligand systems so that data available for comparison are sparse. Of the three group 4 transition metals, only $D_0(Ti^+–N)$ = 5.19 ± 0.13 eV has been directly determined, in a guided ion beam study of the reaction of Ti^+ with NH_3.[29] Clemmer *et al.* combined this bond energy with that for the neutral, $D_0(TiN)$ = 4.93 ± 0.35 eV,[118] and IE(Ti) = 6.82812 eV[41] to determine IE(TiN) = 6.56 ± 0.37 eV, nearly the same as the atom and in agreement with the rough value measured by Stearns and Kohl using high temperature mass spectrometry (HTMS), 6 ± 2 eV.[118] This relationship is also obtained for Th, where IE(ThN) and IE(Th) differ by only 0.02 eV.[15] For Zr and Hf, BDEs of the neutral mononitrides have been determined by HTMS as $D_0(Zr–N)$ = 5.81 ± 0.26 eV by Gingerich[119] and $D_0(Hf–N)$ = 5.50 ± 0.31 eV by Kohl and Stearns,[120] in rough agreement with the estimated value of Gingerich of 6.1 eV.[37] Gingerich also determined the ionization energy of ZrN as IE(ZrN) = 7.9 ± 0.4 eV, which is much larger than IE(Zr) = 6.634 12 ± 0.000 06 eV[121] and leads to $D_0(Zr^+–N)$ = 4.5 ± 0.5 eV. This bond energy is suspect, however, given the similar values of IE(M) and IE(MN) for both Ti and Th, consistent with removing a nonbonding electron. Assuming that IE(M) − IE(MN) remains similar between all four metals, then the IE(M) − IE(MN) for M = Zr and Hf can be estimated conservatively as the average between the differences for Ti and Th: 0.13 ± 0.17 eV. Using this value, ZrN and HfN bond energies can be estimated as $D_0(Zr^+–N)$ = 5.94 ± 0.31 eV and $D_0(Hf^+–N)$ = 5.63 ± 0.35 eV (Table VII). For Ti, Zr, and Th, these various bond energies agree with lower limits obtained by the observation of the reactions $M^+ + N_2O \rightarrow MN^+ + NO$, indicating $D(M^+–N) > D_0(N–NO)$ = 4.925 eV.[34] For Hf, this reaction is not observed, but this could be because Hf^+ has a $^2D(5d6s^2)$ configuration such that the filled 6s orbital lessens the reactivity.[122] These BDEs also agree with upper limits obtained by the failure to observe the reactions $M^+ + NO \rightarrow MN^+ + O$, indicating $D(M^+–N) < D_0(N–O)$ = 6.50 eV.[123]

Notably, MCH^+ and MN^+ for the group 4 transition metals and thorium are isoelectronic, and the BDEs of MCH^+ have been measured in guided ion beam studies of the reactions of the atomic ions with methane.[16,122,124,125] For comparison, the MCH^+ BDEs are also listed in Table VII and Fig. 5. For both M = Ti and Th, the MCH^+ BDEs are very similar to the measured MN^+ BDEs. Thus, $D_0(Zr^+–CH)$ = 5.96 ± 0.22 eV and $D_0(Hf^+–CH)$ = 5.10 ± 0.15 eV indicate that the ZrN^+ and HfN^+ BDEs estimated here are reasonable.

The trend of BDEs for the group 4 transition metals and Th is similar to the trend observed for other ligands (O and CH),[16–18] as shown in Fig. 5. The dissociation energy generally increases moving down the group as would be expected from the lanthanide/actinide contraction. The exception is Hf^+, which has BDEs closer to those

TABLE VII. A comparison of ML^+ (L = N, CH, O) BDEs (eV).

M	Ti	Zr	Hf	Th	U
$D_0(M^+–N)$	5.19 ± 0.13[a]	5.94 ± 0.31[b]	5.63 ± 0.35[c]	6.51 ± 0.08[d]	4.7 ± 0.2[e]
$D_0(M^+–CH)$	5.25 ± 0.17[a,f]	5.96 ± 0.22[g]	5.10 ± 0.15[h]	6.19 ± 0.16[i]	
$D_0(M^+–O)$	6.88 ± 0.07[j]	7.76 ± 0.11[k]	6.91 ± 0.11[l]	8.57 ± 0.14[m]	8.02 ± 0.14[n]

[a]Reference 29.
[b]Calculated from neutral BDE (Ref. 119) and the estimated difference IE(MN) — IE(M) = 0.13 ± 0.17 eV, as discussed in the text.
[c]Calculated from neutral HfN BDE using estimate from Ref. 120 and the estimated difference in IE (see note b).
[d]This work.
[e]Reference 33.
[f]Reference 124.
[g]Reference 125.
[h]Reference 122.
[i]Reference 16.
[j]Reference 130.
[k]Reference 131.
[l]Reference 132.
[m]Reference 18.
[n]Reference 13.

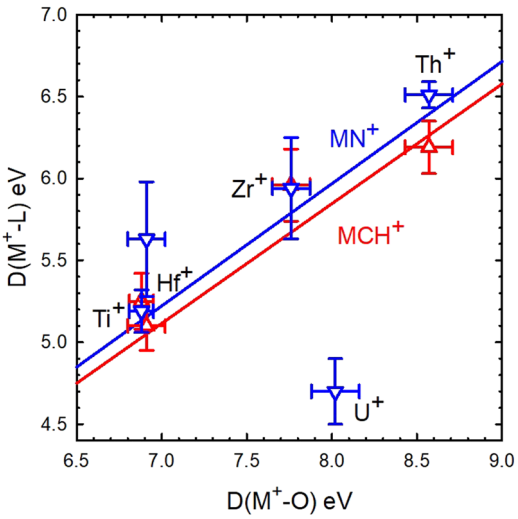

FIG. 5. Correlation of ML^+ bond dissociation energies for the group 4 transition metals, thorium, and uranium and L = O, CH, and N. Values are taken from Table VII. Lines are linear regression analyses of the data constrained to pass through the origin.

of Ti^+ rather than exceeding those of Zr^+ because Hf^+ has a doubly occupied frontier orbital in its $^2D_{3/2}$ ($5d6s^2$) ground electronic state, unlike those of Ti^+ and Zr^+ that have a $^4F_{3/2}$, d^2s ground state configuration, and Th^+, which is a mixture of the $^4F_{3/2}$ and $^2D_{3/2}$ levels.[16–18] Thus, the promotion energy required to form the covalent bonds in these molecules is larger for Hf than for the other three metal cations, weakening its BDEs.

Figure 5 also includes this comparison for UO^+ and UN^+, where it can be seen that the latter value is much smaller than what might be expected on the basis of the other metals. As the thermochemistry for UO^+ is reasonably well established, a reinvestigation of the UN^+ bond energy (obtained in an early ion beam experiment)[33] may be warranted; however, an alternative explanation for this lower BDE is discussed in the section titled "Estimation of actinide nitride bond dissociation energies."

Estimation of actinide nitride bond dissociation energies

BDEs of the actinide nitrides are not readily available. UN^+ was observed in ion beam experiments in the reaction of U^+ with N_2 by Armentrout *et al.*[33] where they determined $D_0(U^+–N) = 4.7 \pm 0.2$ eV. Later in FT-ICR experiments at thermal energies reported by Heinemann and Schwarz,[126] UN^+ was observed in reactions with N_2O with a branching ratio of 30/70 UN^+/UO^+. The same report examined the reactions of UN^+ with several oxidants including O_2 and CO_2. Products formed were $NUO^+ + O/CO$ (33%/25%), $UO^+ + NO$ (24%), and $UO_2^+ + N/CN$ (43%/75%), indicating lower and upper limits to the UN^+ BDE of 4.925 eV ≤ $D_0(U^+–N)$ ≤ 9.80 eV. On the basis of the previous ion beam experiments, Heinemann and Schwarz concluded that the UN^+ BDE was likely close to the lower limit of 5 eV. Later, UN^+ and NpN^+, in addition to ThN^+, were observed in reactions with N_2O in FT-ICR experiments reported by Santos *et al.*[5] with AnN^+/AnO^+ branching ratios of 40/60 and 25/75, respectively, and in agreement with Heinemann and Schwarz. The failure to observe AnN^+ in corresponding reactions with NO infers that an upper limit of $D_0(An^+–N) \le D_0(N–O) = 6.50$ eV can be established for UN^+ and NpN^+. The failure to observe AnN^+ for all actinides other than Th^+, U^+, and Np^+ in this and subsequent reports[11,127] indicates an upper limit of $D_0(An^+–N) \le D_0(ON–N) = 4.925$ eV. To the best of our knowledge, gas phase determinations of neutral AnN thermochemical values are limited to ThN and UN.

Unfortunately, the lack of experimental data makes it hard to project nitride thermochemistry throughout the actinide series. Nevertheless, a simple model may predict AnN^+ BDEs. Previously, Gibson has reported that LnO^+ and AnO^+ BDEs are correlated with the promotion energy of the ground state Ln^+/An^+ to the first state with a $5d^2/6d^2$ configuration.[6] Such a configuration allows the Ln^+/An^+ ion to form a triple bond with O by the O donating four $2p$ electrons and the Ln^+/An^+ donating two $5d/6d$ electrons. Because the $5f$ electrons play a minimal role in the oxide bonding, Gibson proposed an intrinsic AnO^+ BDE (L = O), $D_0(An^+–O)^*$,

$$D_0\left(An^+ - L\right)^* = D_0\left(An^+ - L\right) + E_p\left(6d^2\right), \tag{11}$$

where $E_p(6d^2)$ is the promotion energy of An^+ from the ground state to the first state with a $6d^2$ configuration. Notably, for Th^+, $E_p(6d^2) = 0$ eV so that $D_0(An^+–O)^* \approx D_0(Th^+–O)$ and the ThO^+ BDE can be used to predict the AnO^+ BDEs for the remaining An series.

DFT and higher order calculations for Th and U species indicate that orbital structure remains relatively constant between carbides, nitrides, and oxides.[10,18] Presumably, the simple model in Eq. (11) could potentially be extended to predict AnN^+ BDEs; however, the tables of Blaise and Wyart[54] indicate that, unlike Th^+, states with $6d^3$ configurations are not readily available for the remaining An^+. Therefore, unlike the triple bond of ThN^+, the remaining AnN^+ likely have a bond order of 2.5 where the N donates three $2p$ electrons and An^+ again donates the two $6d$ electrons. Consequently, a better estimate of $D_0(An^+–N)^*$ may be the diabatic BDE of the ThN^+ ($^3\Sigma^+$) state that can form directly from ground state Th^+ (^{4}F, $6d^27s$) + N (^{4}S). This BDE can be estimated from the ground state BDE by utilizing the estimated excitation energy of the ThN^+ $^1\Sigma^+$ state to the $^3\Sigma^+$ state $E^*(^3\Sigma^+) = 1.31 \pm 0.19$ eV, calculated from the values in Table II, which results in $D_0(Th^+–N, {}^3\Sigma^+) \approx D_0(An^+–N)^* = 5.20 \pm 0.21$ eV.

The estimated BDEs of AnN^+ from Eq. (11) with L = N are presented in Table VIII. A comparison to the available experimental data for UN^+ and NpN^+ are also presented in Table VIII. The estimated UN^+ BDE is in good agreement with the previously reported ion beam value of 4.7 ± 0.2 eV; however, the estimated value is lower than $D_0(N–NO)$. Given the FT-ICR results, this suggests that the model in Eq. (11) underestimates the true BDE of UN^+. This discrepancy is also observed in the estimated BDE of NpN^+. Nevertheless, given the large discrepancies reported in DFT calculated BDEs,[14] Eq. (11) model may represent a reasonable and computationally inexpensive estimate of AnN^+ BDEs in the absence of experimental results.

TABLE VIII. AnN^+ BDEs (in eV) estimated using the intrinsic BDE model in Eq. (11) with comparison to experimental values.

AnN^+	AnN^{+*}[a]	AcN^+	PaN^+	UN^+	NpN^+	PuN^+	AmN^+	CmN^+
$E_p(6d^2)$[b]		1.64	0.59	0.57	0.9 ± 0.4[c]	2.14	3.6 ± 0.2[c]	1.84
$D_0(An^+–N)$[d]	5.20 ± 0.21[a]	3.56 ± 0.21	4.61 ± 0.21	4.63 ± 0.21	4.30 ± 0.45	3.06 ± 0.21	1.60 ± 0.29	3.36 ± 0.21
Experimental				4.7 ± 0.2[e]	≥4.92[f]			
				≥4.92[f,g]				

[a]The intrinsic BDE of AnN^+ for the actinide series estimated as the diabatic BDE of ThN^+ ($^3\Sigma^+$) calculated using $D_0(Th^+–N)$ = 6.51 ± 0.08 eV and the estimated excitation energy from ThN^+ ($^1\Sigma^+$) to ThN^+ ($^3\Sigma^+$), $E^*(^3\Sigma^+)$ = 1.31 ± 0.19 eV. See text.
[b]Promotion energy from the ground state to the first state with two 6*d* electrons. Unless noted otherwise, all energies are taken from the tables of Blaise and Wyart (Ref. 54).
[c]Reference 13 and supplementary material.
[d]Estimated AnN^+ BDE calculated using Eq. (11). See text.
[e]Reference 33.
[f]Reference 5.
[g]Reference 3.

CONCLUSION

Analysis of the kinetic energy dependence of the cross section from reaction (7) (Fig. 1) and reaction (10) (Fig. 2) gives thresholds providing consistent values of $D_0(Th^+–N)$. Combining the two results leads to our final value of 6.51 ± 0.08 eV. The only literature thermochemistry on ThN^+ available for comparison comes from combining the precisely known IEs of Th and ThN with a ThN BDE extrapolated from high temperature mass spectrometry experiments, yielding $D_0(Th^+–N)$ = 5.92 ± 0.35 eV, somewhat below the present value. It seems likely that the discrepancy arises from the choice of parameters used to extrapolate data from high temperatures to 0 K for $D_0(Th–N)$, which can be a significant source of error as noted by Murad and Hildenbrand.[128,129] Therefore, we combine the present value of $D_0(Th^+–N)$ with IE(Th) and IE(ThN) to provide a refined value for $D_0(ThN)$ of 6.53 ± 0.08 eV. We also find that $D_0(Th^+–N)$ is larger than its transition metal cation congeners, Ti^+, Zr^+, and Hf^+, consistent with the result expected because of the actinide contraction.

In general, approximate quantum chemical calculations provide ThN^+ BDEs in reasonable agreement with the experiment once spin-orbit corrections using a semiempirical approach are included. In particular, complete basis set extrapolations generally yield good results. The most advanced computational approach used here, FPD composite calculations, leads to BDEs for both ThN^+ and ThN in excellent agreement with our experimental value, further validating the FPD approach as an accurate method for calculating actinide thermochemical values.

ACKNOWLEDGMENTS

This work was supported by the Heavy Element Chemistry Program, Office of Basic Energy Sciences, U. S. Department of Energy, through Grant Nos. DE-SC0012249 (P.B.A.) and DE-SC0008501 (K.A.P.). R.M.C. and P.B.A. also thank the Center for High Performance Computing at the University of Utah for the generous allocation of computer time.

The authors declare no competing financial interest.

REFERENCES

[1]P. B. Armentrout and J. L. Beauchamp, "Collision induced dissociation of UO^+ and UO_2^+," Chem. Phys. **50**, 21–25 (1980).
[2]P. B. Armentrout and J. L. Beauchamp, "Reactions of U^+ and UO^+ with O_2, CO, CO_2, COS, CS_2 and D_2O," Chem. Phys. **50**, 27–36 (1980).
[3]H. H. Cornehl, R. Wesendrup, M. Diefenbach, and H. Schwarz, "A comparative study of oxo-ligand effects in the gas-phase chemistry of atomic lanthanide and actinide cations," Chem.–Eur. J. **3**, 1083–1090 (1997).
[4]J. K. Gibson and R. G. Haire, "Gas-phase chemistry of bare and oxo-ligated protactinium ions: A contribution to a systematic understanding of actinide chemistry," Inorg. Chem. **41**, 5897–5906 (2002).
[5]M. Santos, J. Marçalo, A. P. d. Matos, J. K. Gibson, and R. G. Haire, "Gas-phase oxidation reactions of neptunium and plutonium ions investigated via Fourier transform ion cyclotron resonance mass spectrometry," J. Phys. Chem. A **106**, 7190–7194 (2002).
[6]J. K. Gibson, "Role of atomic electronics in f-element bond formation: Bond energies of lanthanide and actinide oxide molecules," J. Phys. Chem. A **107**, 7891–7899 (2003).
[7]M. Santos, J. Marçalo, J. P. Leal, A. P. d. Matos, J. K. Gibson, and R. G. Haire, "FTICR-MS study of the gas-phase thermochemistry of americium oxides," Int. J. Mass Spectrom. **228**, 457–465 (2003).
[8]J. K. Gibson, R. G. Haire, M. Santos, J. Marçalo, and A. P. d. Matos, "Oxidation studies of dipositive actinide ions, An^{2+} (An = Th, U, Np, Pu, Am) in the gas phase: Synthesis and characterization of the isolated uranyl, neptunyl, and plutonyl ions UO_2^{2+}(g), NpO_2^{2+}(g), and PuO_2^{2+}(g)," J. Phys. Chem. A **109**, 2768–2781 (2005).
[9]V. Goncharov and M. C. Heaven, "Spectroscopy of the ground and low-lying excited states of ThO^+," J. Chem. Phys. **124**, 064312 (2006).
[10]M. C. Heaven, "Probing actinide electronic structure using fluorescence and multi-photon ionization spectroscopy," Phys. Chem. Chem. Phys. **8**, 4497–4509 (2006).
[11]J. K. Gibson, R. G. Haire, J. Marçalo, M. Santos, J. P. Leal, A. Pires de Matos, R. Tyagi, M. K. Mrozik, R. M. Pitzer, and B. E. Bursten, "FTICR/MS studies of gas-phase actinide ion reactions: Fundamental chemical and physical properties of atomic and molecular actinide ions and neutrals," Eur. Phys. J. D **45**, 133–138 (2007).
[12]J. K. Gibson, R. G. Haire, J. Marçalo, M. Santos, A. Pires de Matos, M. K. Mrozik, R. M. Pitzer, and B. E. Bursten, "Gas-phase reactions of hydrocarbons with An^+ and AnO^+ (An = Th, Pa, U, Np, Pu, Am, Cm): The active role of 5f electrons in organoprotactinium chemistry," Organometallics **26**, 3947–3956 (2007).
[13]J. Marçalo and J. K. Gibson, "Gas-phase energetics of actinide oxides: An assessment of neutral and cationic monoxides and dioxides from thorium to curium," J. Phys. Chem. A **113**, 12599–12606 (2009).

[14]C. C. L. Pereira, C. J. Marsden, J. Marçalo, and J. K. Gibson, "Actinide sulfides in the gas phase: Experimental and theoretical studies of the thermochemistry of AnS (An = Ac, Th, Pa, U, Np, Pu, Am and Cm)," Phys. Chem. Chem. Phys. **13**, 12940–12958 (2011).
[15]M. C. Heaven, B. J. Barker, and I. O. Antonov, "Spectroscopy and structure of the simplest actinide bonds," J. Phys. Chem. A **118**, 10867–10881 (2014).
[16]R. M Cox, P. B. Armentrout, and W. A. de Jong, "Activation of CH_4 by Th^+ as studied by guided ion beam mass spectrometry and quantum chemistry," Inorg. Chem. **54**, 3584–3599 (2015).
[17]R. M Cox, P. B. Armentrout, and W. A. de Jong, "Reactions of Th^+ + H_2, D_2, and HD studied by guided ion beam tandem mass spectrometry and quantum chemical calculations," J. Phys. Chem. B **120**, 1601–1614 (2016).
[18]R. M Cox, M. Citir, P. B. Armentrout, S. R. Battey, and K. A. Peterson, "Bond energies of ThO^+ and ThC^+: A guided ion beam and quantum chemical investigation of the reactions of thorium cation with O_2 and CO," J. Chem. Phys. **144**, 184309 (2016).
[19]G. Mazzone, M. d. C. Michelini, N. Russo, and E. Sicilia, "Mechanistic aspects of the reaction of Th^+ and Th^{2+} with water in the gas phase," Inorg. Chem. **47**, 2083–2088 (2008).
[20]K. J. d. Almeida and H. A. Duarte, "Gas-phase methane activation by the Ac^+–Pu^+ ions: Theoretical insights into the role of 5f electrons/orbitals in early actinide chemistry," Organometallics **28**, 3203–3211 (2009).
[21]E. Di Santo, M. d. C. Michelini, and N. Russo, "Methane C–H bond activation by gas-phase Th^+ and U^+: Reaction mechanisms and bonding analysis," Organometallics **28**, 3716–3726 (2009).
[22]I. Infante, A. Kovacs, G. L. Macchia, A. R. M. Shahi, J. K. Gibson, and L. Gagliardi, "Ionization energies for the actinide mono- and dioxides series, from Th to Cm: Theory versus experiment," J. Phys. Chem. A **114**, 6007–6015 (2010).
[23]J. Zhou and H. B. Schlegel, "*Ab initio* molecular dynamics study of the reaction between Th^+ and H_2O," J. Phys. Chem. A **114**, 8613–8617 (2010).
[24]K. J. de Almeida and H. A. Duarte, "Dehydrogenation of methane by gas-phase Th, Th^+, and Th^{2+}: Theoretical insights into actinide chemistry," Organometallics **29**, 3735–3745 (2010).
[25]A. Kovács and R. J. M. Konings, "Computed vibrational frequencies of actinide oxides $AnO^{0/+/2+}$ and $AnO_2^{0/+/2+}$ (An = Th, Pa, U, Np, Pu, Am, Cm)," J. Phys. Chem. A **115**, 6646–6656 (2011).
[26]B. B. Averkiev, M. Mantina, R. Valero, I. Infante, A. Kovacs, D. G. Truhlar, and L. Gagliardi, "How accurate are electronic structure methods for actinoid chemistry?," Theor. Chem. Acc. **129**, 657–666 (2011).
[27]E. Goos, A. Burcat, and B. Ruscic, Extended Third Millennium Ideal Gas and Condensed Phase Thermochemical Database for Combustion with Updates from Active Thermochemical Tables; ANL-05/20 and TAE 960 Technion-IIT, Aerospace Engineering, and Argonne National Laboratory, Chemistry Division, 2016.
[28]D. E. Clemmer, L. S. Sunderlin, and P. B. Armentrout, "Ammonia activation by V^+: Electronic and translational energy dependence," J. Phys. Chem. **94**, 208–217 (1990).
[29]D. E. Clemmer, L. S. Sunderlin, and P. B. Armentrout, "Ammonia activation by Sc^+ and Ti^+: Electronic and translational energy dependence," J. Phys. Chem. **94**, 3008–3015 (1990).
[30]M. T. Rodgers, B. Walker, and P. B. Armentrout, "Reactions of Cu^+(^{1}S and ^{3}D) with O_2, CO, CO_2, NO, N_2O, and NO_2 studied by guided ion beam mass spectrometry," Int. J. Mass Spectrom. **182-183**, 99–120 (1999).
[31]L. Tan, F. Liu, and P. B. Armentrout, "Thermochemistry of the activation of N_2 on iron cluster cations: Guided ion beam studies of the reactions of Fe_n^+ (n = 1–19) with N_2," J. Chem. Phys. **124**, 084302-1–084302-14 (2006).
[32]F. Liu, M. Li, L. Tan, and P. B. Armentrout, "Guided ion beam studies of the reactions of Co_n^+ (n = 1–18) with N_2: Cobalt cluster mononitride and dinitride bond energies," J. Chem. Phys. **128**, 194313-1–194313-12 (2008).
[33]P. B. Armentrout, R. V. Hodges, and J. L. Beauchamp, "Endothermic reactions of uranium ions with N_2, D_2 and CD_4," J. Chem. Phys. **66**, 4683–4688 (1977).
[34]V. V. Lavrov, V. Blagojevic, G. K. Koyanagi, G. Orlova, and D. K. Bohme, "Gas-phase oxidation and nitration of first-, second-, and third-row atomic cations in reactions with nitrous oxide: Periodicities in reactivity," J. Phys. Chem. A **108**, 5610–5624 (2004).
[35]G. K. Koyanagi and D. K. Bohme, "Oxidation reactions of lanthanide cations with N_2O and O_2: Periodicities in reactivity," J. Phys. Chem. A **105**, 8964–8968 (2001).
[36]R. Johnsen, F. R. Castell, and M. A. Biondi, "Rate coefficients for oxidation of Ti^+ and Th^+ by O_2 and NO at low energies," J. Chem. Phys. **61**, 5404–5407 (1974).
[37]K. A. Gingerich, "Gaseous metal nitrides. III. On the dissociation energy of thorium mononitride and predicted dissociation energies of diatomic group III–VI transition-metal nitrides," J. Chem. Phys. **49**, 19–24 (1968).
[38]G. P. Kushto, P. F. Souter, and L. Andrews, "An infrared spectroscopic and quasirelativistic theoretical study of the coordination and activation of dinitrogen by thorium and uranium atoms," J. Chem. Phys. **108**, 7121–7130 (1998).
[39]A. T. Le, S. G. Nakhate, D.-T. Nguyen, T. C. Steimle, and M. C. Heaven, "Characterization of gas-phase thorium nitride," J. Chem. Phys. **150**, 144304 (2019).
[40]S. Kohler, R. Deissenberger, K. Eberhardt, N. Erdmann, G. Herrmann, G. Huber, J. V. Kratz, M. Nunnemann, G. Passler, P. M. Rao, J. Riegel, N. Trautmann, and K. Wendt, "Determination of the first ionization potential of actinide elements by resonance ionization mass spectroscopy," Spectrochim. Acta, Part B **52B**, 717–726 (1997).
[41]J. E. Sansonetti and W. C. Martin, "Handbook of basic atomic spectroscopic data," J. Phys. Chem. Ref. Data **34**, 1559–2259 (2005).
[42]S. K. Loh, D. A. Hales, L. Lian, and P. B. Armentrout, "Collision-induced dissociation of Fe_n^+ (n = 2–10) with Xe: Ionic and neutral iron cluster binding energies," J. Chem. Phys. **90**, 5466–5485 (1989).
[43]R. H. Schultz and P. B. Armentrout, "Reactions of N_4^+ with rare gases from thermal to 10 eV c.m.: Collision-induced dissociation, charge transfer, and ligand exchange," Int. J. Mass Spectrom. Ion Processes **107**, 29–48 (1991).
[44]E. Teloy and D. Gerlich, "Integral cross sections for ion-molecule reactions. 1. The guided beam technique," Chem. Phys. **4**, 417–427 (1974).
[45]P. B. Armentrout, "The kinetic energy dependence of ion-molecule reactions: Guided ion beams and threshold measurements," Int. J. Mass Spectrom. **200**, 219–241 (2000).
[46]K. M. Ervin and P. B. Armentrout, "Translational energy dependence of Ar^+ + XY → ArX^+ + Y (XY = H_2, D_2, HD) from thermal to 30 eV c.m," J. Chem. Phys. **83**, 166–189 (1985).
[47]P. J. Chantry, "Doppler broadening in beam experiments," J. Chem. Phys. **55**, 2746–2759 (1971).
[48]R. M Cox and P. B. Armentrout, "Activation of water by thorium cation: A guided ion beam and quantum chemical study," J. Am. Soc. Mass Spectrom. (in press).
[49]C. L. Haynes and P. B. Armentrout, "Thermochemistry and structures of $CoC_3H_6^+$: Metallacycle and metal-alkene isomers," Organometallics **13**, 3480–3490 (1994).
[50]D. E. Clemmer, Y.-M. Chen, F. A. Khan, and P. B. Armentrout, "State-specific reactions of Fe^+(a^6D, a^4F) with D_2O and reactions of FeO^+ with D_2," J. Phys. Chem. **98**, 6522–6529 (1994).
[51]B. L. Kickel and P. B. Armentrout, "Reactions of Fe^+, Co^+ and Ni^+ with silane. Electronic state effects and M^+-SiH_x (x = 0–3) bond energies," J. Am. Chem. Soc. **117**, 764–773 (1995).
[52]B. L. Kickel and P. B. Armentrout, "Guided ion beam studies of the reactions of group 3 metal ions (Sc^+, Y^+, La^+, and Lu^+) with silane. Electronic state effects, comparison to reactions with methane, and M^+-SiH_x (x = 0–3) bond energies," J. Am. Chem. Soc. **117**, 4057–4070 (1995).
[53]M. R. Sievers, Y.-M. Chen, J. L. Elkind, and P. B. Armentrout, "Reactions of Y^+, Zr^+, Nb^+, and Mo^+ with H_2, HD, and D_2," J. Phys. Chem. **100**, 54–62 (1996).
[54]See http://web2.lac.u-psud.fr/lac/Database/Contents.html for "Energy Levels and Atomic Spectra of Actinides".
[55]W. J. Chesnavich and M. T. Bowers, "Theory of translationally driven reactions," J. Phys. Chem. **83**, 900–905 (1979).
[56]F. Muntean and P. B. Armentrout, "Guided ion beam study of collision-induced dissociation dynamics: Integral and differential cross sections," J. Chem. Phys. **115**, 1213–1228 (2001).
[57]N. Aristov and P. B. Armentrout, "Reaction mechanisms and thermochemistry of V^+ + C_2H_{2p} (p = 1,2,3)," J. Am. Chem. Soc. **108**, 1806–1819 (1986).

[58]M. E. Weber, J. L. Elkind, and P. B. Armentrout, "Kinetic energy dependence of $Al^+ + O_2 \rightarrow AlO^+ + O$," J. Chem. Phys. **84**, 1521–1529 (1986).
[59]M. J. Frisch, G. W. Trucks, H. B. Schlegel, G. E. Scuseria, M. A. Robb, J. R. Cheeseman, G. Scalmani, V. Barone, B. Mennucci, G. A. Petersson, H. Nakatsuji, M. Caricato, X. Li, H. P. Hratchian, A. F. Izmaylov, J. Bloino, G. Zheng, J. L. Sonnenberg, M. Hada, M. Ehara, K. Toyota, R. Fukuda, J. Hasegawa, M. Ishida, T. Nakajima, Y. Honda, O. Kitao, H. Nakai, T. Vreven, J. A. Montgomery, Jr., J. E. Peralta, F. Ogliaro, M. J. Bearpark, J. Heyd, E. N. Brothers, K. N. Kudin, V. N. Staroverov, R. Kobayashi, J. Normand, K. Raghavachari, A. P. Rendell, J. C. Burant, S. S. Iyengar, J. Tomasi, M. Cossi, N. Rega, N. J. Millam, M. Klene, J. E. Knox, J. B. Cross, V. Bakken, C. Adamo, J. Jaramillo, R. Gomperts, R. E. Stratmann, O. Yazyev, A. J. Austin, R. Cammi, C. Pomelli, J. W. Ochterski, R. L. Martin, K. Morokuma, V. G. Zakrzewski, G. A. Voth, P. Salvador, J. J. Dannenberg, S. Dapprich, A. D. Daniels, Ö. Farkas, J. B. Foresman, J. V. Ortiz, J. Cioslowski, and D. J. Fox, GAUSSIAN 09, Revision D.01, Gaussian, Inc., Wallingford, CT, USA, 2009.
[60]K. A. Peterson, "Correlation consistent basis sets for actinides. I. The Th and U atoms," J. Chem. Phys. **142**, 074105 (2015).
[61]A. Weigand, X. Cao, T. Hangele, and M. Dolg, "Relativistic small-core pseudopotentials for actinium, thorium, and protactinium," J. Phys. Chem. A **118**, 2519–2530 (2014).
[62]W. Küchle, M. Dolg, H. Stoll, and H. Preuss, "Energy-adjusted pseudopotentials for the actinides. Parameter sets and test calculations for thorium and thorium monoxide," J. Chem. Phys. **100**, 7535–7542 (1994).
[63]X. Cao and M. Dolg, "Segmented contraction scheme for small-core actinide pseudopotential basis sets," J. Mol. Struct.: THEOCHEM **673**, 203–209 (2004).
[64]T. H. Dunning, "Gaussian basis sets for use in correlated molecular calculations. I. The atoms boron through neon and hydrogen," J. Chem. Phys. **90**, 1007–1023 (1989).
[65]R. A. Kendall, T. H. Dunning, and R. J. Harrison, "Electron affinities of the first-row atoms revisited. Systematic basis sets and wave functions," J. Chem. Phys. **96**, 6796–6806 (1992).
[66]K. A. Peterson and T. H. Dunning, "Accurate correlation consistent basis sets for molecular core–valence correlation effects: The second row atoms Al–Ar, and the first row atoms B–Ne revisited," J. Chem. Phys. **117**, 10548–10560 (2002).
[67]R. Krishnan, J. S. Binkley, R. Seeger, and J. A. Pople, "Self-consistent molecular orbital methods. XX. A basis set for correlated wave functions," J. Chem. Phys. **72**, 650–654 (1980).
[68]A. Karton and J. M. L. Martin, "Comment on: 'Estimating the Hartree–Fock limit from finite basis set calculations' [Jensen F (2005) Theor Chem Acc 113:267]," Theor. Chem. Acc. **115**, 330–333 (2006).
[69]J. M. L. Martin, "*Ab initio* total atomization energies of small molecules—Towards the basis set limit," Chem. Phys. Lett. **259**, 669–678 (1996).
[70]L. Andrews, Y. Gong, B. Liang, V. E. Jackson, R. Flamerich, S. Li, and D. A. Dixon, "Matrix infrared spectra and theoretical studies of thorium oxide species: ThO_x and Th_2O_y," J. Phys. Chem. A **115**, 14407–14416 (2011).
[71]L. Andrews, K. S. Thanthiriwatte, X. Wang, and D. A. Dixon, "Thorium fluorides ThF, ThF_2, ThF_3, ThF_4, $ThF_3(F_2)$, and ThF_5—Characterized by infrared spectra in solid argon and electronic structure and vibrational frequency calculations," Inorg. Chem. **52**, 8228–8233 (2013).
[72]K. S. Thanthiriwatte, X. Wang, L. Andrews, D. A. Dixon, J. Metzger, T. Vent-Schmidt, and S. Riedel, "Properties of ThF_x from infrared spectra in solid argon and neon with supporting electronic structure and thermochemical calculations," J. Phys. Chem. A **118**, 2107–2119 (2014).
[73]A. D. Becke, "Density-functional thermochemistry. III. The role of exact exchange," J. Chem. Phys. **98**, 5648–5652 (1993).
[74]C. Lee, W. Yang, and R. G. Parr, "Development of the Colle-Salvetti correlation-energy formula into a functional of the electron density," Phys. Rev. B **37**, 785–789 (1988).
[75]J. P. Perdew, K. Burke, and Y. Wang, "Generalized gradient approximation for the exchange-correlation hole of a many-electron system," Phys. Rev. B **54**, 16533–16539 (1996).
[76]Y. Zhao and D. G. Truhlar, "The M06 suite of density functionals for main group thermochemistry, thermochemical kinetics, noncovalent interactions, excited states, and transition elements: Two new functionals and systematic testing of four M06-class functionals and 12 other functionals," Theor. Chem. Acc. **120**, 215–241 (2008).
[77]C. Adamo and V. Barone, "Toward reliable density functional methods without adjustable parameters: The PBE0 model," J. Chem. Phys. **110**, 6158–6170 (1999).
[78]E. Di Santo, M. C. Michelini, and N. Russo, "Activation of ethane C–H and C–C bonds by gas phase Th^+ and U^+: A theoretical study," J. Phys. Chem. A **113**, 14699–14705 (2009).
[79]X. Zhang and H. Schwarz, "Bonding in cationic MCH_2^+ (M=K–La, Hf–Rn): A theoretical study on periodic trends," Chem.–Eur. J. **16**, 5882–5888 (2010).
[80]G. D. Purvis and R. J. Bartlett, "A full coupled-cluster singles and doubles model: The inclusion of disconnected triples," J. Chem. Phys. **76**, 1910–1918 (1982).
[81]J. A. Pople, M. Head-Gordon, and K. Raghavachari, "Quadratic configuration interaction. A general technique for determining electron correlation energies," J. Chem. Phys. **87**, 5968–5975 (1987).
[82]G. E. Scuseria, C. L. Janssen, and H. F. Schaefer, "An efficient reformulation of the closed-shell coupled cluster single and double excitation (CCSD) equations," J. Chem. Phys. **89**, 7382–7387 (1988).
[83]G. E. Scuseria and H. F. Schaefer III, "Is coupled cluster singles and doubles (CCSD) more computationally intensive than quadratic configuration interaction (QCISD)?," J. Chem. Phys. **90**, 3700–3703 (1989).
[84]J. B. Foresman and A. E. Frisch, *Exploring Chemistry with Electronic Structure Methods*, 2nd ed. (Gaussian, Inc., Pittsburgh, PA, 1996).
[85]M. A. Garcia and M. D. Morse, "Resonant two-photon ionization spectroscopy of jet-cooled OsN: 520–418 nm," J. Chem. Phys. **135**, 114304 (2011).
[86]P. B. Armentrout, "The bond energy of ReO^+: Guided ion-beam and theoretical studies of the reaction of Re^+ (^7S) with O_2," J. Chem. Phys. **139**, 084305 (2013).
[87]P. B. Armentrout and F.-X. Li, "The bond energy of IrO^+: Guided ion-beam and theoretical studies of the reaction of Ir^+ (^5F) with O_2," J. Phys. Chem. A **117**, 7754–7766 (2013).
[88]D. Feller, K. A. Peterson, and D. A. Dixon, "A survey of factors contributing to accurate theoretical predictions of atomization energies and molecular structures," J. Chem. Phys. **129**, 204105 (2008).
[89]M. Vasiliu, K. A. Peterson, J. K. Gibson, and D. A. Dixon, "Reliable potential energy surfaces for the reactions of H_2O with ThO_2, PaO_2^+, UO_2^{2+}, and UO_2^+," J. Phys. Chem. A **119**, 11422–11431 (2015).
[90]R. Feng and K. A. Peterson, "Correlation consistent basis sets for actinides. II. The atoms Ac and Np–Lr," J. Chem. Phys. **147**, 084108 (2017).
[91]M. Douglas and N. M. Kroll, "Quantum electrodynamical corrections to the fine structure of helium," Ann. Phys. **82**, 89–155 (1974).
[92]M. Reiher and A. Wolf, "Exact decoupling of the Dirac Hamiltonian. II. The generalized Douglas-Kroll-Hess transformation up to arbitrary order," J. Chem. Phys. **121**, 10945–10956 (2004).
[93]W. A. de Jong, R. J. Harrison, and D. A. Dixon, "Parallel Douglas-Kroll energy and gradients in NWChem: Estimating scalar relativistic effects using Douglas-Kroll contracted basis sets," J. Chem. Phys. **114**, 48–53 (2001).
[94]G. E. Scuseria, "The open-shell restricted Hartree-Fock singles and doubles coupled-cluster method including triple excitations CCSD(T): Application to the carbon triatomic monopositive ion," Chem. Phys. Lett. **176**, 27–35 (1991).
[95]J. D. Watts, J. Gauss, and R. J. Bartlett, "Coupled-cluster methods with non-iterative triple excitations for restricted-open-shell-Hartree-Fock and other general single-determinant reference functions. Energies and analytical gradients," J. Chem. Phys. **98**, 8718–8733 (1993).
[96]P. J. Knowles, C. Hampel, and H. J. Werner, "Coupled custer theory for high spin, open shell reference wave functions," J. Chem. Phys. **99**, 5219–5227 (1993).
[97]H.-J. Werner, P. J. Knowles, G. Knizia, F. R. Manby, M. Schutz, P. Celani, T. Korona, R. Lindh, A. Mitrushenkov, G. Rauhut, K. R. Shamasundar, T. B. Adler, R. D. Amos, A. Bernhardsson, A. Berning, D. L. Cooper, M. J. O. Deegan, A. J. Dobbyn, F. Eckert, E. Goll, C. Hampel, A. Hesselmann, G. Hertzer, T. Hrenar, G. Jansen, C. Koppl, Y. Liu, A. W. Lloyd, R. A. Mata, A. J. May, S. J. McNicholas, W. Meyer, M. E. Mura, A. Nicklass, D. P. O'Neill, P. Palmieri, D. Peng, K. Pflüger, R. Pitzer, M. Reiher, T. Shiozaki, H. Stoll, A. J. Stone, R. Tarroni, T. Thorsteinsson,

and M. Wang, MOLPRO, version 2012.1, a package of *ab initio* programs, 2012, see http://www.molpro.net.
[98]Y. C. Park, I. S. Lim, and Y. S. Lee, "Two-component spin-orbit effective core potential calculations with an all-electron relativistic program DIRAC," Bull. Korean Chem. Soc. **33**, 803–808 (2012).
[99]L. Visscher, T. J. Lee, and K. G. Dyall, "Formulation and implementation of a relativistic unrestricted coupled-cluster method including noniterative connected triples," J. Chem. Phys. **105**, 8769–8776 (1996).
[100]K. G. Dyall, "An exact separation of the spin-free and spin-dependent terms of the Dirac-Coulomb-Breit Hamiltonian," J. Chem. Phys. **100**, 2118–2127 (1994).
[101]T. Saue, L. Visscher, H. J. Aa. Jensen, and R. Bast, with contributions from V. Bakken, K. G. Dyall, S. Dubillard, U. Ekström, E. Eliav, T. Enevoldsen, E. Faßhauer, T. Fleig, O. Fossgaard, A. S. P. Gomes, T. Helgaker, J. Henriksson, M. Iliaš, Ch. R. Jacob, S. Knecht, S. Komorovský, O. Kullie, C. V. Larsen, J. K. Lærdahl, Y. S. Lee, H. S. Nataraj, P. Norman, G. Olejniczak, J. Olsen, Y. C. Park, J. K. Pedersen, M. Pernpointner, R. di Remigio, K. Ruud, P. Sałek, B. Schimmelpfennig, J. Sikkema, A. J. Thorvaldsen, J. Thyssen, J. van Stralen, S. Villaume, O. Visser, T. Winther, and S. Yamamoto, DIRAC, a relativistic *ab initio* electronic structure program, Release DIRAC14 (2014), 2014.
[102]K. G. Dyall, C. W. Bauschlicher, D. W. Schwenke, and P. Pyykko, "Is the Lamb shift chemically significant?," Chem. Phys. Lett. **348**, 497–500 (2001).
[103]P. Pyykko and L.-B. Zhao, "Search for effective local model potentials for simulation of quantum electrodynamic effects in relativistic calculations," J. Phys. B: At., Mol. Opt. Phys. **36**, 1469–1478 (2003).
[104]J. Noga and R. J. Bartlett, "The full CCSDT model for molecular electronic structure," J. Chem. Phys. **86**, 7041–7050 (1987).
[105]J. D. Watts and R. J. Bartlett, "The coupled-cluster single, double, and triple excitation model for open-shell single reference functions," J. Chem. Phys. **93**, 6104–6105 (1990).
[106]S. A. Kucharski and R. J. Bartlett, "Recursive intermediate factorization and complete computational linearization of the coupled-cluster single, double, triple, and quadruple excitation equations," Theor. Chim. Acta **80**, 387–405 (1991).
[107]N. Oliphant and L. Adamowicz, "Multireference coupled-cluster method using a single-reference formalism," J. Chem. Phys. **94**, 1229–1235 (1991).
[108]S. A. Kucharski and R. J. Bartlett, "The coupled-cluster single, double, triple, and quadruple excitation method," J. Chem. Phys. **97**, 4282–4288 (1992).
[109]M. Kállay and P. R. Surján, "Higher excitations in coupled-cluster theory," J. Chem. Phys. **115**, 2945–2954 (2001).
[110]A. MRCC, *String-Based Quantum Chemical Program Suite* (University of Technology and Economics, Budapest, 2001).
[111]T. Su, "Parameterization of kinetic energy dependences of ion-polar molecule collision rate constants by trajectory calculations," J. Chem. Phys. **100**, 4703 (1994).
[112]E. W. Rothe and R. B. Bernstein, "Total collision cross sections for the interactions of atomic beams of alkali metals with gases," J. Chem. Phys. **31**, 1619–1627 (1959).
[113]J. D. Burley, K. M. Ervin, and P. B. Armentrout, "Translational energy dependence of $O^+(^4S) + H_2(D_2, HD) \rightarrow OH^+(OD^+) + H(D)$ from thermal to 30 eV c.m," Int. J. Mass Spectrom. Ion Processes **80**, 153–175 (1987).
[114]S. L. Redman, G. Nave, and C. J. Sansonetti, "The spectrumm of thorium from 250 nm TO 5500 nm: Ritz wavelengths and optimized energy levels," Astrophys. J., Suppl. Ser. **211**, 4–12 (2014).
[115]D. H. Bross, J. G. Hill, H.-J. Werner, and K. A. Peterson, "Explicitly correlated composite thermochemistry of transition metal species," J. Chem. Phys. **139**, 094302 (2013).
[116]L. Cheng, J. Gauss, B. Ruscic, P. B. Armentrout, and J. F. Stanton, "Bond dissociation energies for diatomic molecules containing 3d transition metals: Benchmark scalar-relativistic coupled-cluster calculations for twenty molecules," J. Chem. Theory Comput. **13**, 1044–1056 (2017).
[117]Z. Fang, M. Vasiliu, K. A. Peterson, and D. A. Dixon, "Prediction of bond dissociation energies/heats of formation for diatomic transition metal compounds: CCSD(T) works," J. Chem. Theory Comput. **13**, 1057–1066 (2017).
[118]C. A. Stearns and F. J. Kohl, "The dissociation energy of gaseous titanium mononitride," High Temp. Sci. **2**, 146–153 (1970); NASA technical note D-5027, Springfield, VA (1969).
[119]K. A. Gingerich, "Gaseous metal nitrides. II. The dissociation energy, heat of sublimation, and heat of formation of zirconium mononitride," J. Chem. Phys. **49**, 14–18 (1968).
[120]F. J. Kohl and C. A. Stearns, "Identification and dissociation energy of gaseous hafnium mononitride," J. Phys. Chem. **78**, 273–274 (1974).
[121]S. Hasegawa and D. Nagamoto, "Two-color laser resonance ionization spectroscopy of zirconium atoms," J. Phys. Soc. Jpn. **86**, 104302 (2017).
[122]L. G. Parke, C. S. Hinton, and P. B. Armentrout, "Why is hafnium so unreactive? Experimental and theoretical studies of the reaction of Hf^+ with methane," Int. J. Mass Spectrom. **254**, 168–182 (2006).
[123]V. Blagojevic, E. Flaim, M. J. Y. Jarvis, G. K. Koyanagi, and D. K. Bohme, "Nitric oxide as an electron donor, an atom donor, an atom acceptor, and a ligand in reactions with atomic transition-metal and main-group cations in the gas phase," J. Phys. Chem. A **109**, 11224–11235 (2005).
[124]L. S. Sunderlin and P. B. Armentrout, "Methane activation by Ti^+: Electronic and translational energy dependence," J. Phys. Chem. **92**, 1209–1219 (1988).
[125]P. B. Armentrout and M. R. Sievers, "Activation of CH_4 by gas-phase Zr^+ and the thermochemistry of Zr ligand complexes," J. Phys. Chem. A **107**, 4396–4406 (2003).
[126]C. Heinemann and H. Schwarz, "NUO^+, a new species isoelectronic to the uranyl dication UO," Chem.–Eur. J. **1**, 7–11 (1995).
[127]J. K. Gibson, R. G. Haire, M. Santos, A. P. d. Matos, and J. Marçalo, "Gas-phase oxidation of Cm^+ and Cm^{2+}—Thermodynamics of neutral and ionized CmO," J. Phys. Chem. A **112**, 11373–11381 (2008).
[128]D. L. Hildenbrand and E. Murad, "Mass spectrometric studies of gaseous ThO and ThO_2," J. Chem. Phys. **61**, 1232–1237 (1974).
[129]J. B. Pedley and E. M. Marshall, "Thermochemical data for gaseous monoxides," J. Phys. Chem. Ref. Data **12**, 967–1031 (1983).
[130]D. E. Clemmer, J. L. Elkind, N. Aristov, and P. B. Armentrout, "Reaction of Sc^+, Ti^+, and V^+ with CO. MC^+ and MO^+ bond energies," J. Chem. Phys. **95**, 3387–3393 (1991).
[131]M. R. Sievers, Y.-M. Chen, and P. B. Armentrout, "Metal oxide and carbide thermochemistry of Y^+, Zr^+, Nb^+, and Mo^+," J. Chem. Phys. **105**, 6322–6333 (1996).
[132]C. S. Hinton, F.-X. Li, and P. B. Armentrout, "Reactions of Hf^+, Ta^+, and W^+ with O_2 and CO: Metal carbide and metal oxide cation bond energies," Int. J. Mass Spectrom. **280**, 226–234 (2009).